

Petri Sulasalmi

MODELLING OF SLAG
EMULSIFICATION AND
SLAG REDUCTION
IN CAS-OB PROCESS

UNIVERSITY OF OULU GRADUATE SCHOOL;
UNIVERSITY OF OULU,
FACULTY OF TECHNOLOGY



ACTA UNIVERSITATIS OULUENSIS
C Technica 592

PETRI SULASALMI

**MODELLING OF SLAG
EMULSIFICATION AND SLAG
REDUCTION IN CAS-OB PROCESS**

Academic dissertation to be presented with the assent of the Doctoral Training Committee of Technology and Natural Sciences of the University of Oulu for public defence in the Arina auditorium (TA105), Linnanmaa, on 2 December 2016, at 12 noon

UNIVERSITY OF OULU, OULU 2016

Copyright © 2016
Acta Univ. Oul. C 592, 2016

Supervised by
Professor Timo Fabritius
Assistant Professor Mika Järvinen

Reviewed by
Assistant Professor Mikael Ersson
Professor Hans-Jürgen Odenthal

Opponent
Professor Seppo Louhenkilpi

ISBN 978-952-62-1415-3 (Paperback)
ISBN 978-952-62-1416-0 (PDF)

ISSN 0355-3213 (Printed)
ISSN 1796-2226 (Online)

Cover Design
Raimo Ahonen

JUVENES PRINT
TAMPERE 2016

Sulasalmi, Petri, Modelling of slag emulsification and slag reduction in CAS-OB process.

University of Oulu Graduate School; University of Oulu, Faculty of Technology

Acta Univ. Oul. C 592, 2016

University of Oulu, P.O. Box 8000, FI-90014 University of Oulu, Finland

Abstract

Composition Adjustment by Sealed argon bubbling – Oxygen Blowing (CAS-OB) process is a ladle treatment process that was developed for chemical heating and alloying of steel. The main stages of the process are heating, (possible) alloying and reduction of slag. The CAS-OB process aims for homogenization and control of the composition and temperature of steel.

In this dissertation, a mathematical reaction model was developed for the slag reduction stage of the CAS-OB process. Slag reduction is carried out by applying vigorous bottom stirring from porous plugs at the bottom of the ladle. Due to the bottom stirring a circular steel flow is induced which disrupts top slag layer and due to shear stress at the steel-slag interface small slag droplets are detached. This induces an immense increase in the interfacial area between steel and slag which provides favourable conditions for the reduction reactions. In order to model reduction reactions, a sub-model for describing the interfacial area was needed. For this the slag droplet formation was studied using computational fluid dynamics (CFD) and based on these studies, a sub-model for droplet formation was developed. The model for the reduction stage of the CAS-OB process takes into account not only the reaction during the reduction but also the heat transfer between the phases, ladle and surroundings.

The reduction stage model was validated using validation data obtained from the CAS-OB station of the SSAB Raabe steel plant in Finland. It was concluded that the model was able to predict steel and slag compositions as well as the steel temperature very well.

Keywords: CAS-OB, CFD, emulsification of slag, mathematical modelling, slag reduction

Sulasalmi, Petri, Kuonan pisaroitumisen ja kuonan pelkistyksen mallinnus CAS-OB -prosessissa.

Oulun yliopiston tutkijakoulu; Oulun yliopisto, Teknillinen tiedekunta

Acta Univ. Oul. C 592, 2016

Oulun yliopisto, PL 8000, 90014 Oulun yliopisto

Tiivistelmä

CAS-OB -prosessi on sulametallurgiassa käytettävä senkkäkäsittelyprosessi, joka on kehitetty teräksen kemialliseen lämmittämiseen ja seostukseen. CAS-OB-prosessin pääprosessivaiheet ovat lämmitysvaihe, mahdollinen seostusvaihe ja kuonan pelkistysvaihe. CAS-OB -prosessilla tavoitellaan teräksen koostumuksen homogenisointiin ja lämpötilan kontrollointiin.

Tässä tutkimuksessa kehitettiin matemaattinen reaktiomalli CAS-OB -prosessin kuonan pelkistysvaiheen kuvaamiseen. Kuonan pelkistys tapahtuu senkan pohjassa olevien huuhtelutiilien avulla suoritettavan voimakkaan kaasuhuuhtelun avulla. Pohjahuuhtelu aiheuttaa kiertävän teräsvirtauksen senkassa. Teräsvirtaus irrottaa teräksen päällä olevasta kuonakerroksesta pisaroita ja kuonan ja teräksen välinen reaktiopinta-ala kasvaa voimakkaasti. Tämä tarjoaa suotuisat olosuhteet pelkistysreaktiolle senkassa. Pelkistysreaktioiden mallintamiseksi tässä työssä kehitettiin CFD-simulaatioiden avulla alimalli, jonka avulla voidaan kuvata teräksen ja kuonan välisen pinta-alan suuruutta. Pelkistysvaiheen mallissa huomioidaan reaktioiden lisäksi myös systeemissä tapahtuva lämmösiirto.

Pelkistysmalli validoitiin mittausdatalla, joka hankittiin SSAB Raahen terässulaton CAS-OB -asemalla järjestetyssä validointikampanjassa. Tutkimuksessa havaittiin, että malli kykenee hyvin ennustamaan teräksen ja kuonan koostumuksen sekä teräksen lämpötilan.

Asiasanat: CAS-OB, CFD, kuonan emulgoituminen, kuonan pelkistys, matemaattinen mallinnus

Acknowledgements

The study presented in this work was mainly funded by the Finnish Funding Agency for Technology and Innovation (Tekes) under the AMMe project of the Energy and Lifecycle Efficient Metal Processes (ELEMET) program and Showcase 2.1 of the System Integrated Metal Production (SIMP) program. At the very beginning of my research, considerable funding was received from the FEMA project. Metallinjalostajien rahasto awarded a research grant for finalizing the thesis. Furthermore, this thesis was supported by smaller grants from the Jenny and Antti Wihuri Foundation, Walter Ahlström Foundation and Tauno Tönning Foundation. I would like to sincerely thank the aforementioned for making this work possible.

When I began working at the Process Metallurgy Research Unit in 2007, which at the time was the Laboratory of Process Metallurgy, as a Master's thesis worker I wasn't planning to make a doctoral thesis. After finalizing my Master's degree I was given the opportunity to continue as a researcher. Compared to many other researchers I was fortunate to be able to concentrate on the same research topic, the modelling of slag emulsification, for a quite long period of time. Eventually, publications came along and the idea of putting them together and making a doctoral thesis arose. Applying the results of the emulsification studies in the modelling of the reduction stage of the CAS-OB process nailed down the topic of my thesis. A lot of people were there to help me carry out the planning of the studies and to write the articles. First of all I would like to thank my supervisors Professor Timo Fabritius and Professor Mika Järvinen for sharing their deep knowledge with me and for their support and encouragement throughout the work. Secondly, my deepest gratitude goes to my closest colleagues, Mr. Ville-Valtteri Visuri and Mr. Aki Kärnä for the fertile collaboration and good discussions, work-related and otherwise. Without you guys I wouldn't have been able to finalize this thesis. Furthermore, I want to thank Mr. Jari Savolainen from Outokumpu Stainless and Mr. Seppo Ollila from SSAB Raahe. The starting point of my work was based on the physical modelling carried out by Mr. Savolainen. Mr. Ollila provided invaluable help and knowledge when the validation data was collected in the SSAB Raahe steelplant. I would also like to thank my pre-examiners Professor Hans-Jürgen Odenthal and Professor Mikael Ersson for their excellent comments that definitely improved this thesis. Furthermore, I would like to thank other colleagues in the Process

Metallurgy Reseach Unit, especially Dr. Antti Kemppainen and Dr. Hannu Suopajarvi for exploring the culinary art in Oulu with me.

I would like to express my deepest gratitude to my family and friends. I want to thank my parents for their support my whole life which has been essential for me to get this far. Finally, I want to thank my partner Sanna and our children Auku and Iisa for your love and support.

List of original publications

This thesis is based on the following publications, which are referred throughout the text by their Roman numerals:

- I Sulasalmi P, Kärnä A, Fabritius T & Savolainen J (2009) CFD Model for Emulsification of Slag into the Steel. *ISIJ Int* 42(11): 1661–1667.
- II Sulasalmi P, Visuri V-V & Fabritius T (2013) Effect of Interfacial Tension on the Emulsification of Slag – Considerations on the CFD Modelling of Dispersion. *Mater Sci Forum* 762: 242–247.
- III Sulasalmi P, Visuri V-V, Kärnä A & Fabritius T (2015) Simulation of the Effect of Steel Flow Velocity on Slag Droplet Distribution and Interfacial Area Between Steel and Slag. *Steel Res Int* 86(3): 212–222.
- IV Sulasalmi P, Visuri V-V, Kärnä A, Järvinen M, Ollila S & Fabritius T (2016) A Mathematical Model for the Reduction Stage of the CAS-OB Process. *Metall and Materi Trans B*. DOI: 10.1007/s11663-016-0769-8.

All the publications were written by the author of this thesis. The author's main responsibilities were the development of the mathematical models, carrying out the calculations and reporting the results.

Contents

Abstract	
Tiivistelmä	
Acknowledgements	7
List of original publications	9
Contents	11
1 Introduction	13
1.1 Objective of the work	13
2 The CAS-OB process	17
3 State of the art	21
3.1 The emulsification of slag	21
3.1.1 Physical modelling	22
3.1.2 Mathematical modelling	30
4 Description of the models	41
4.1 Modelling of emulsification of slag	41
4.1.1 The Volume Of Fluid method (VOF)	42
4.1.2 The Large Eddy Simulation model (LES)	43
4.2 The slag reduction model of the CAS-OB process	48
4.2.1 The reaction system and the governing equations in the model	50
4.2.2 The emulsification module for the reduction stage model of the CAS-OB process	54
4.2.3 The activity of the species	56
4.2.4 Mass and heat transfer coefficients	57
4.2.5 The physical properties of the phases	60
4.2.6 Validation of the models	62
5 Results and discussion	65
5.1 Slag emulsification	65
5.1.1 The effect of physical properties	65
5.1.2 The effect of interfacial tension	67
5.1.3 The effect of steel flow velocity	68
5.2 The reduction stage model	71
5.2.1 Steel and slag compositions	71

6 Conclusions and future work	75
References	77
Original publications	81

1 Introduction

The CAS-OB process is a ladle treatment process in secondary metallurgy which is used for the chemical heat-up of steel. Under certain circumstances molten steel cannot be shifted immediately from the converter to the casting. This may be due to a jam in the caster or the steel may need to be alloyed to ensure desired composition. This delay causes cooling of the molten steel. The CAS-OB process can be employed to ensure sufficient temperature of the steel before casting. During the heat-up stage aluminium is burned on the surface of steel under a ceramic bell using oxygen blowing by supersonic lance. Aluminum oxide formed during the heating goes into the slag phase lying on top of the steel surface and some amount of aluminium is dissolved into the steel.

Due to the intensive lance blowing, in addition to aluminum, some portion of other metals from the steel phase, Mn, Si and Fe in particular, are oxidized into the slag. This is undesirable from the economical point of view and, thus, is usually necessary to perform *slag reduction* after the heat-up stage. In the slag reduction stage, the steel phase is strongly stirred by blowing some inert gas, usually Argon, from the bottom of the ladle. The gas stirring forces the steel phase into a circular motion. At the interface of steel and slag, the flowing steel causes the disengagement of small droplets from the top slag layer. The slag droplets and steel form an *emulsion* where a large interfacial area between phases occurs. The increased interfacial area accelerates the mass transfer between the steel and slag and, hence, provides preferable conditions for reduction reactions. In order to model fundamental phenomena during slag reduction it is essential to provide a model for the slag emulsification.

1.1 Objective of the work

The main objective in this work was to develop a mathematical reaction model for the slag reduction stage of the CAS-OB process. With the model, the composition of steel, slag and gas phases, as well as the steel temperature, can be predicted in a transient manner. In order to describe the mass and heat transfer during the process stage in question, a submodel for the slag emulsification had to be created. The slag emulsification phenomenon was studied by way of Computational Fluid Dynamics (CFD). The droplet formation during bottom stirring is affected by numerous factors. According to Cramb and Jimbo [1] interfacial tension between steel and slag is the most

important property that determines emulsification. In addition, the density difference, slag viscosity and the velocity of steel have to be accounted for in order to describe the phenomenon properly. Although comprehensive understanding of all aspects of droplet formation is yet to be achieved, many studies have been carried out to enlighten the subject. Available studies include physical modelling [2–5], mathematical modelling [6–9], as well as industrial level and phenomena related studies [1, 10, 11]. In this thesis a review of the available studies is included, as well as a thorough description of our attempt to model slag emulsification.

The developed reduction stage model consists of several submodels, including the aforementioned emulsification model, an activity model of the species in different phases, models for the mass and heat transfer coefficients and models for the physical properties etc. Three original papers in this thesis concern the modelling of slag emulsification and one paper presents the reduction stage model of the CAS-OB process. The content of the original papers is presented in Table 1. Table 1 presents the assembly of the reduction stage model and how the original papers are related to it.

A rather small number of published studies are available regarding the modelling of CAS-OB process. The reduction stage model of CAS-OB presented in this thesis is the first of its kind that has ever been published. Our previous work introduced a model for the heat-up stage [19]. One aim of developing the reduction stage model was to extend the previous model towards a comprehensive process model.

Table 1. The original papers.

Paper	Contents
I	Simulation of slag emulsification in oil-water based on physical modelling. Simulation of slag-steel cases. The main interest was on the effect of viscosity, layer width of the upper phase and interfacial tension on the droplet formation.
II	Simulation of a slag-steel system. Further developed model for studying the effect of interfacial tension between slag and steel on slag emulsification.
III	Simulation of a slag-steel system for studying the effect of flow velocity of steel to slag emulsification.
IV	A mathematical model for calculating chemical reactions and heat transfer in the slag reduction stage of the CAS-OB process.

Reduction stage model of the CAS-OB process

PAPER IV

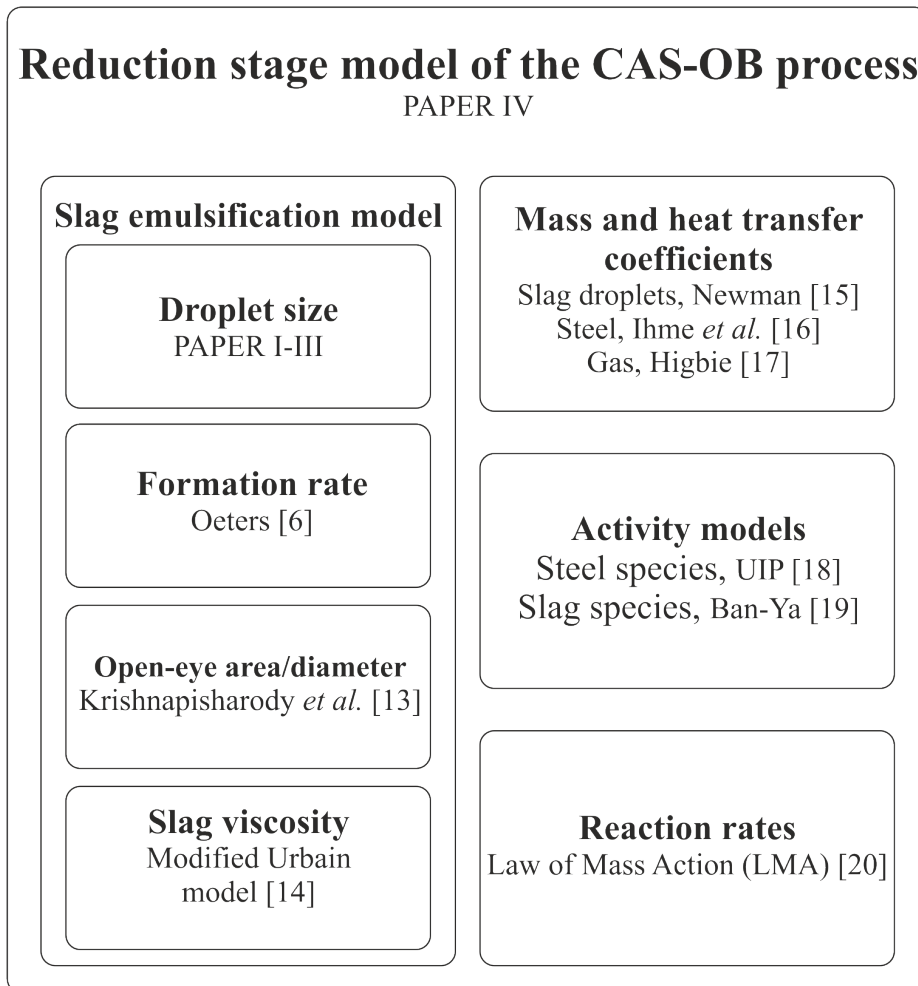


Fig. 1. Composition of the CAS-OB process model.

2 The CAS-OB process

Since the objective of this thesis is to model a particular process stage of the CAS-OB process, a brief overview of the secondary metallurgy, chemical heating and the CAS-OB process itself is necessary.

In order to make it economic, modern steel making is divided into a primary step and secondary step. Production of basic steel in an oxygen converter process or the electric arc furnace constitutes the primary step. The primary step is followed by the tapping of the steel into a ladle. For producing high-quality steel, all further treatments before casting take place in the ladle. This is called secondary metallurgy [20].

The CAS-OB process is a ladle treatment process developed for the chemical heating of steel. The abbreviation CAS-OB stands for **C**omposition **A**djustment by **S**ealed Argon bubbling - **O**xygen **B**lowing. The process was developed and patented by Nippon Steel Corporation in the 1980s. There are number of tasks that must be covered in secondary metallurgy. As for the CAS-OB process, the most important functions are the adjustment of the temperature to an optimum level and the accurate addition of alloying elements. The purpose of the heating is to ensure sufficient temperature of the melt when it is supplied to the caster. The CAS-OB process belongs among the processes that operate at atmospheric pressure [20, 21]. According to Stolte [20] the following advantages are achieved as a result of using the CAS-OB process:

- Decrease in tapping temperature of appr. 15 °C
- Less re-blowing of the BOF heats
- Fast and reliable homogenization of alloys
- Enables alloying with narrow tolerances
- Reduced alloy consumption and costs
- Low total oxygen content after treatment
- Less aborted heats
- Buffering between BOF and casting resulting in improved teeming conditions.

In chemical heating processes the steel is heated by way of an exothermic reaction of a dissolved element by oxygen blowing. The use of aluminium is preferred as an element for chemical heating. It has been reported that a concentration of 0.1% of dissolved aluminium within the melt is able to produce a temperature rise of +34 °C by reacting

with oxygen gas [20]. Obviously, there are also heat losses caused by radiation and through the ladle walls.

The CAS-OB process is presented schematically in Fig. 2, the equipment is similar to that used in SSAB Europe Raahe. The equipment consists of a refractory bell which is connected to a lifting system. A pipe connected to the alloying and dedusting system is positioned above the bell. In addition, the pipe provides a route for taking samples and temperature measurements. The upper part of the bell is coated with a castable refractory material from the inside. The lower part is protected externally as well. Argon is injected through a porous plug at the bottom of the ladle.

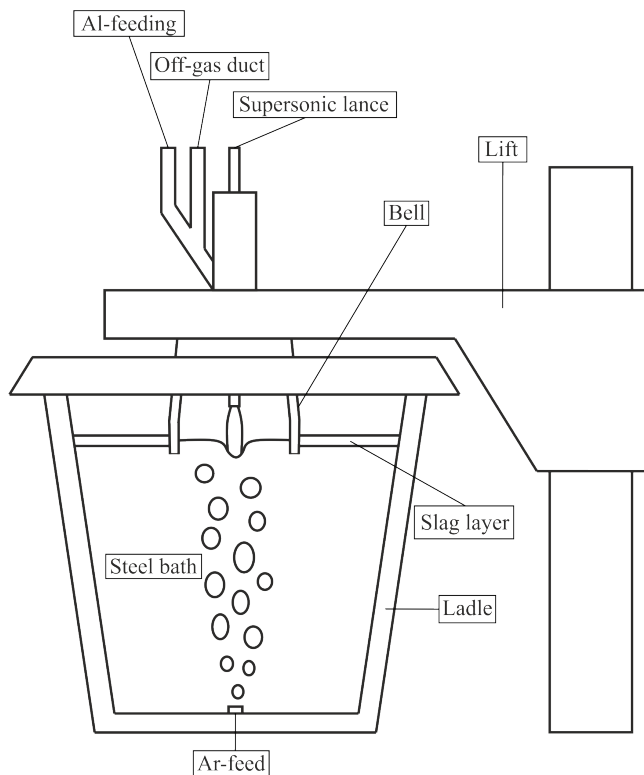


Fig. 2. Schematic of the CAS-OB process at SSAB Raahe.

The procedure of the CAS-OB treatment is started by defining the steel bath level for immersing the bell to sufficient depth. Before the bell is lowered, the Argon flow rate is increased in such a way that a slag-free area, i.e. an open-eye, is formed into which the bell is immersed. After the bell is lowered, the bottom blowing is decreased

and deoxidation of the steel is carried out by Al or Al-Si addition. Depending on the temperature measurement, the deoxidation process is followed by the heating of the steel. In the heat-up stage solid aluminium particles are fed onto the steel surface and oxygen is simultaneously blown via the top lance. A possible alloying stage follows after the heat-up stage has been completed. Steel samples are taken before heating and after alloying just before the bell is lifted.

The CAS-OB process has been subject to a number of studies, most of them are physical modelling or experimental studies [22–25]. Apart from the present study, only a few studies have been carried out on mathematical modelling of the CAS-OB process. [19, 26]

3 State of the art

This chapter reviews some of the main results in the modelling of slag emulsification and process modelling.

3.1 The emulsification of slag

As pointed out in the previous chapter, the emulsification of slag phase has been examined in several studies. The major interest in studying emulsification is not only restricted to the slag reduction perspective but droplet formation has a significant effect on desulphurization and steel purity as well. From the present thesis' point of view, the interest in studying emulsification arises from the need to accurately describe the mass transfer between slag and steel. The mass transfer rate between phases with dilute concentrations satisfies the following equation

$$\dot{m} = kA(c_b - c_i). \quad (1)$$

In Eq. 1, k , A and $(c_b - c_i)$ are the mass transfer coefficient, interfacial area and concentration gradient, respectively. In particular, determining the accurate magnitude of interfacial area A has been proved to be a very challenging task. In a system of two immiscible fluids, in a non-agitated situation defining the interfacial area is quite a trivial task. However, in an agitated situation, e.g. during vigorous bottom stirring in a ladle, specifying magnitude of A is far from trivial and requires extensive research. Studies have been carried out where the product kA , known as a mass-transfer parameter, has been determined by water-model measurement without determining the mass-transfer coefficient k or interfacial area A at all. [27]

Research methods are divided mainly into two parts, physical modelling and mathematical or numerical modelling. In addition to these, experimental and phenomena related research have been published. In this chapter, selected studies from each approach are introduced to survey the main results in the current slag emulsification research.

3.1.1 Physical modelling

The majority of studies involving physical modelling simulate steel-slag system have been carried out by way of water models in which water corresponds to the steel phase and slag phase is represented by suitable lighter liquid, such as different types of oils or cyclohexane etc.

Mietz et al.

Mietz *et al.* performed extensive series of studies [2, 3, 28] to examine mass transfer in ladle processes during bottom stirring. In the part that focuses on droplet formation [2], measurements were carried out from cylindrical vessels corresponding to an 80-t vessel using three different size ratios: 1:7, 1:4 and 1:2.5. Emulsification fractions were measured from each vessel applying different flow rates with centric and eccentric gas injection. For calculating corresponding gas flow rates, similarity between the model and a full-scale vessel was confirmed by the Froude criterion. Applied fluids in the modelling setup consisted of water representing the metal phase and cyclohexane simulating the slag phase.

It was concluded that with centric gas injection the emulsification fraction is strongly increased with an increasing gas flow rate. Contrary to the centric plug placement, eccentric gas injection produced a much lower degree of emulsification. Increasing the flow rate only weakly enlarged the emulsification fraction. The vessel size barely affected the emulsification fraction with eccentric injection whereas in the case of centric placement the differences are clear as can be seen in Fig. 3 (a).

The rate constant of mass transfer for different systems was determined in their second study.[3] Boundary conditions were similar to those of the emulsification study. For the mass transfer measurement they applied iodine as a dissolved substance that was extracted to the slag. The study was carried out in vessels of three different sizes. The dimensionless concentration was determined from several instances of time during the experiment and the rate constant, kA/V_m , was calculated based on the dimensionless concentration. Results are presented in Fig. 3 (b). With both plug placements the rate constant increases when increasing the flow rate. With centric bottom plug placement the increase was quite strong with the Froude number after critical velocity had been reached. With modest flow rates the difference between rate constants with different plug placements was quite small.

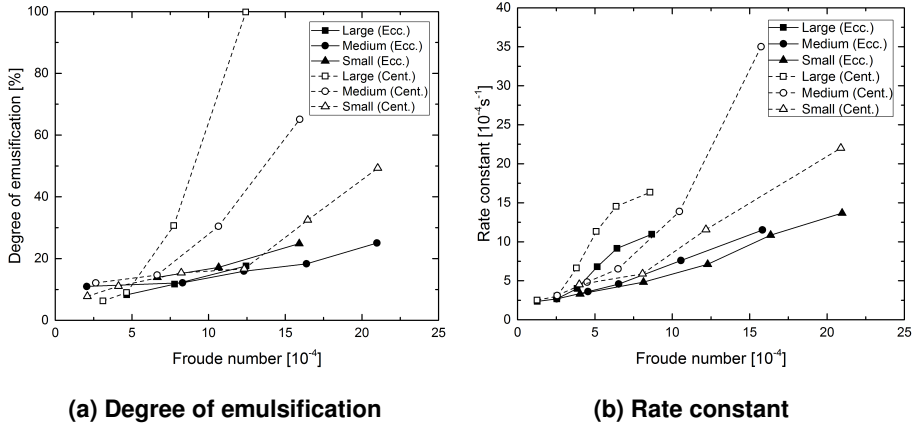


Fig. 3. Emulsification fraction (a) and rate constant (b) as a function of the Froude number. Re-drawn from a figure by Mietz *et al.* [2]

As for the results of the study, Mietz *et al.* conclude that the Froude similarity is not quantitatively sufficient for direct transfer of results to real scale ladles. The reason for this might be that the Froude number does not include the effect of viscosities and interfacial tension. However, the results are applicable for qualitative analysis. For example, the authors concluded that after exceeding a certain critical velocity the degree of emulsification (and mass transfer) increases profusely. Furthermore, they concluded that if strong emulsification is desired, then centric gas injection with sufficiently high gas flow rates should be used. However, excessively high flow rates may have an unfavourable impact because they increase the amount of small droplets which are not able to rise back to the top slag. Thus, owing to the fast saturation, the contribution of the small droplets to the mass transfer is restricted and they may have negative impact on the quality of the end-product.

Frohberg et al.

In determining mass transfer processes between slag and steel - or any immiscible fluids - it is essential to know the magnitude of the transfer area, i.e. the interfacial area between the phases. The moving phase boundary or dispersion of a phase into another makes the description of the mass transfer quite complicated. Frohberg *et al.* [29] investigated the magnitude of the interfacial area under gas-stirring conditions applying a cold modelling approach. In their model, steel was simulated by water

and slag was simulated by parafine oil. The interfacial tension was modified by the addition of alkyphenol. The oil to water ratio was varied as well: the experiments were carried out using ratios of 14%, 22% and 25%. The aim of their work was to measure droplet sizes and estimate mass transfer rates by determining the product kA from the measurements.

Droplet size distributions were determined with a suction probe and an optical system at different gas flow rates and interfacial tensions. It was noticed that lower gas flow rates produced a wider size distribution. When the flow rate was increased the fraction of the droplets in the smaller size classes increased, i.e. the mean diameter decreased. Both the mean diameters and the Sauter mean diameters (SMD) were evaluated. An interesting tendency was noticed when SMD was plotted against flow rate. At lower flow rates, SMD increased and from a certain flow rate onwards it started to decrease. In order to combine the results from several experiments and to include the effect of gas flow rates, interfacial tension and oil fraction, the SMD was plotted against the following parameter

$$P = \frac{\dot{V}}{\sigma^6 (V_o/V_w)^2}. \quad (2)$$

The curve of the following form was fitted to the data

$$d_{32} = c \left(\frac{\dot{V}}{\sigma^6 (V_o/V_w)^2} \right)^{-0.3}, \quad (3)$$

where c is a constant. The resulting plot is presented in Fig. 4.

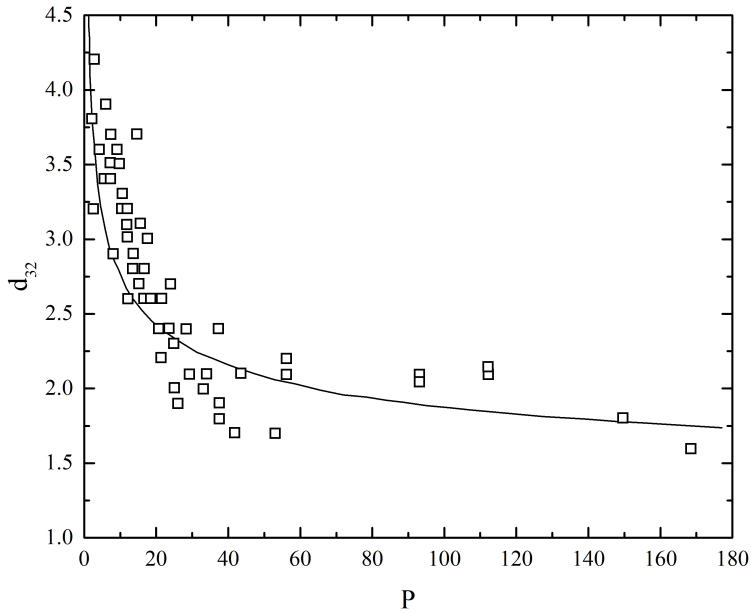


Fig. 4. Sauter mean diameter. The figure was re-drawn after the figure of Frohberg *et al.* [29]

In the second stage, mass transfer rates were evaluated by measuring the change of tracer concentration from the oil-water system under different bottom flow conditions. Caprylic acid served as the tracer and the system was reported to have similar conditions as in the slag-metal reactions. The effect of the number of bottom plugs on the mass transfer rate was reported as well. The product kA was determined according to the following equation

$$\ln(c_w/c_w^0) = \frac{kAt}{V_w}. \quad (4)$$

Fig. 4 presents $\ln(c_w/c_w^0)$ against time which was determined from the measurements with different flow rates. Since t , c_w/c_w^0 and V_w are known, kA can be evaluated by determining the slope of the lines in Fig. 4.

By combining the results from the droplet size measurements and mass transfer experiments the authors determined that the interfacial area with the strongest flow rate (i.e. all the oil is dispersed) is approximately 50 times larger than under non-agitated conditions. They also concluded that there is probably a linear correlation between the gas flow rate and interfacial area.

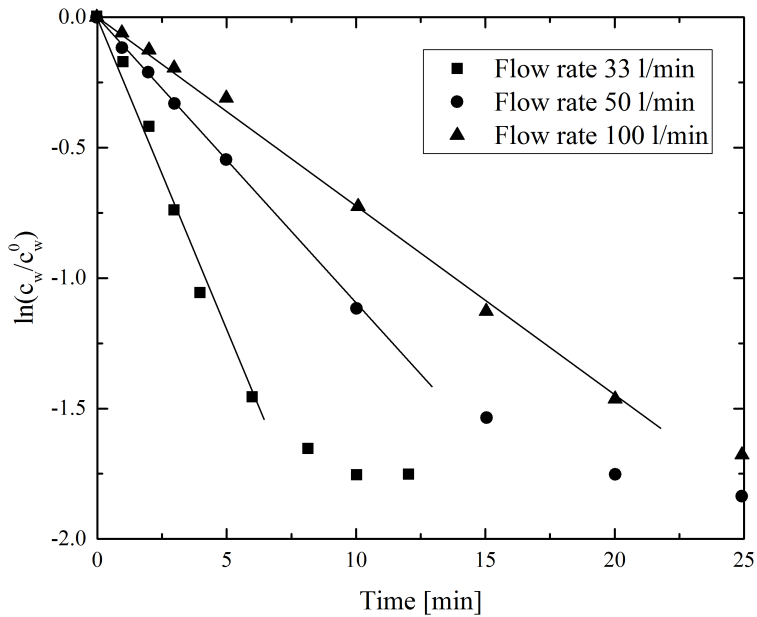


Fig. 5. Dimensionless concentration as a function of time for different flow rates. The figure was re-drawn after the figure of Froberg *et al.* [29]

Savolainen et al.

A study of Savolainen *et al.* [5] aimed at clarifying the effect of different physical properties of fluids on the slag droplet formation with oil-water systems. In their model oil represented the lighter slag phase and water simulated the metal phase. The varied properties included oil viscosity, oil layer thickness, the density difference of phases and the interfacial tension between the oil and water. A schematic drawing of the modelling apparatus used in the measurements is presented in Fig. 6. It can be seen that the fluid flow angle in the apparatus was fixed. The modelling setup formed the basis for the CFD modelling of the present thesis. The main interest in their work was to measure average droplet size under varied conditions. Critical velocities, i.e. the minimum steel flow velocity able to produce perpetual slag emulsification, was determined for each system. Droplet size and velocity measurements were taken from video frames. The interfacial tension was manipulated by using a NaCl-water solution in certain cases. Different types of oil were used to vary the oil viscosity.

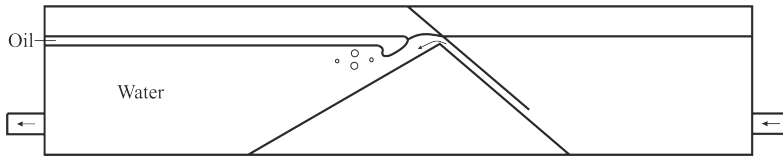


Fig. 6. A schematic drawing of the modelling apparatus used by Savolainen *et al.* [5].

According to the study, when increasing the interfacial tension, oil layer thickness or oil viscosity, the critical velocity increased as well. With increasing interfacial tension or density difference, smaller droplets were produced. As for droplet size, it was concluded that the most dominating factor is the interfacial tension while the slag viscosity was the least significant property. Slag viscosity, in turn, had the greatest effect on the critical velocity, while the thickness of the lighter phase had the smallest impact. The studied systems were analyzed using the modified Weber number and Capillary number. It was concluded that neither of these provided a comprehensive criterion for describing the droplet formation. Furthermore, it was noted that the criterion derived by Xiao *et al.* [30], which states that emulsification can occur when the system satisfies $We > 12.3$, is not a sufficient condition for describing emulsification.

The main results of the study are collected in Table 2. The last column gives a measure of how different properties effect to the critical velocity of emulsification and droplet size.

Khajavi et al.

In a cold model study, Khajavi *et al.* [31] performed measurements in order to quantify droplet size distribution, interfacial area and energy dissipation by way of water-oil systems. The effect of the gas flow rate on the Sauter mean diameter (SMD) of droplets with varying slag layer thickness was observed. Two different oil-water systems, with silicon oil and kerosene, were observed in a bottom-blown cylindrical vessel. In distinction to the work of Frohberg *et al.* [29], with quite similar objectives of investigation, the observed systems were analyzed by a high-speed camera instead of sample taking. The authors criticised sampling for being subject to major problems, such as droplet break-up or coalescence and the discontinuous nature of method which unduly inhibits the detection of samples that are large enough.

Fairly interesting results were reported in regard to SMD behaviour under increasing gas flow rates. In silicon oil-water systems SMD decreased with an increasing flow rate

Table 2. The results of the experiments of Savolainen *et al.* [5].

				Scaled change [%]
Oil layer thickness [m]	0.005	0.01	0.015	
Critical velocity [m/s]	0.29	0.29	0.32	6.72
Average droplet size [mm]	6.75	8.18	8.19	10.66
Oil viscosity [mPa s]	61.34	96.02	149.80	
Critical velocity [m/s]	0.29	0.33	0.36	18.34
Average droplet size [mm]	7.15	6.78	7.150	3.32
Density difference [kg/m ³]	94.00	168.00	266.00	
Critical velocity [m/s]	0.28	0.30	0.36	14.31
Average droplet size [mm]	8.12	7.05	5.64	23.99
Interfacial tension [mN/m]	3.85	4.56	13.04	
Critical velocity [m/s]	0.20	0.22	0.28	16.96
Average droplet size [mm]	3.10	3.91	6.75	49.29

which is consistent to the observation of e.g. Frohberg *et al.* [29]. In a kerosene-water system, instead, increasing gas input had only a minor effect on the SDM with lower rates. Almost no effect at all was observed with higher flow rates. The results are presented in Fig. 7.

The behaviour of interfacial area under different conditions is presented in Fig. 8. The tendency is very clear; the interfacial area increases with gas flow rate and rising thickness of the oil layer. The effect of slag layer thickness is explained by higher pressure at the interface promoting better emulsification. The behaviour in the case of silicon oil, Fig. 8b is notable. When the gas flow rate is increased beyond a certain *critical point*, a sudden leap in the interfacial area occurs. This is due to the entire oil layer breaking into droplets at high flow rates. The interfacial area continues to increase even when the critical point has been exceeded due to further break-up of droplets. This effect does not occur with very thin oil layers or if kerosine serves as the lighter phase.

According to the study, the energy dissipation can be divided into *surface energy* required for the droplet formation and *potential energy* required for maintaining droplets in the other phase. The total energy related to the interfacial phenomena was determined

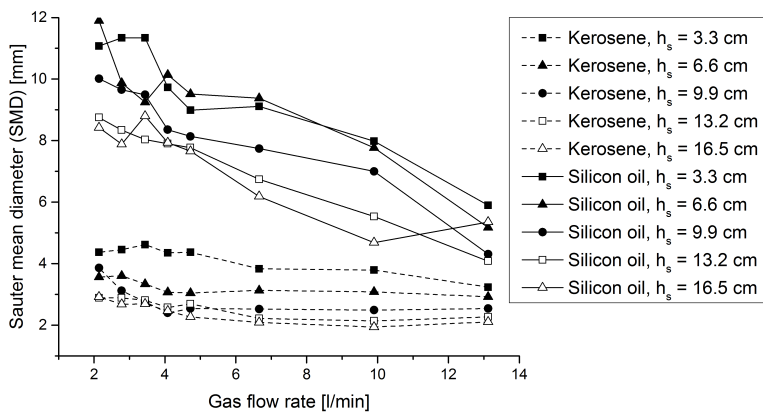


Fig. 7. Sauter mean diameter (SMD) as a function of gas flow rate for different cases. Results were collected into the same figure from data of Khajavi *et al.* [31].

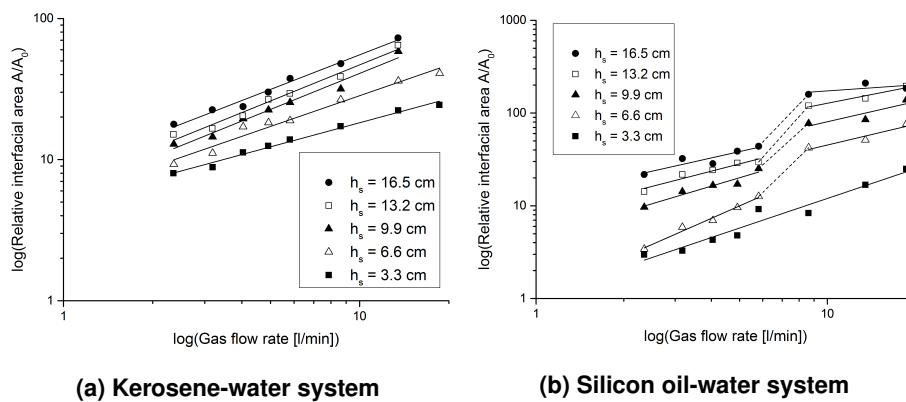


Fig. 8. Interfacial area as a function of gas flow rate in observed systems. Figures were re-drawn from the figures of Khajavi *et al.* [31]

by the following equation

$$E_{i,tot} = \underbrace{A\sigma}_{\text{Surface energy}} + \underbrace{(\rho_m - \rho_s)V_d g \frac{h_{em}}{2}}_{\text{Potential energy}}. \quad (5)$$

In Eq. 5, A , V_d and h_{em} are the interfacial area, total volume of droplets and height of emulsion, respectively. These properties were measured from the experiments for each case. The results for the kerosene-water system and silicon oil-water system regarding total energy are represented in Fig. 9.

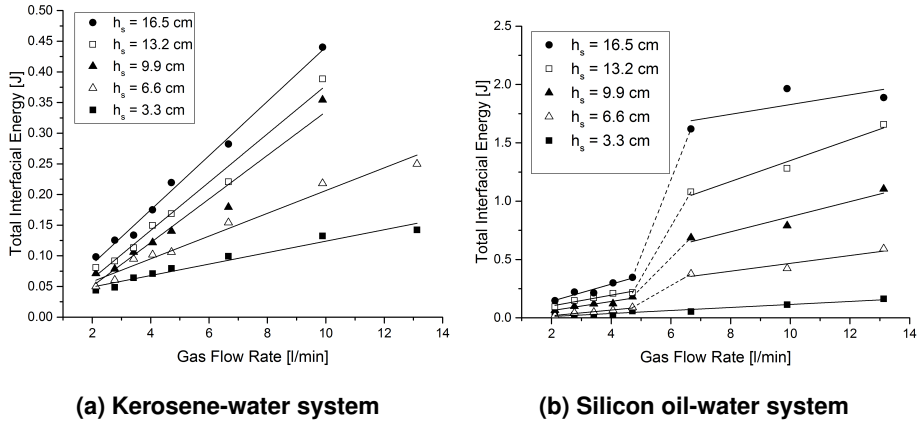


Fig. 9. Total interfacial energy as a function of gas flow rate in observed systems. Figures were re-drawn from the figures of Khajavi *et al.* [31].

3.1.2 Mathematical modelling

In comparison to physical modelling, mathematical modelling has been a far less used approach in modelling of slag emulsification.

Oeters

Oeters[6] suggested a mathematical model for slag emulsification by examination of the force relationship near the slag-metal interface. The model restricts observing the momentum transfer from the down-flowing steel to the slag layer on the edge of an *open-eye* which is formed by rising bubbles due to gas stirring. The model does not take into account the oscillatory movement of the gas bubble plume that would give rise to

periodic changes in force relationships and, thus, affect the droplet size and number of droplets. The subsequent break-up of droplets is omitted from the model as well. The model is reported to have been developed for the emulsification conditions of ladle metallurgy.

The rising gas bubbles due to bottom-blowing carry steel along with them. The gas phase exits the steel bath while the steel flows along the slag interface and is redirected downwards to the bottom of the ladle. The flowing steel transfers momentum to slag phase and causes the slag to accelerate. If the velocity at the slag-steel interface exceeds a *critical velocity*, droplets start to detach from the lower edge of the slag layer. The droplet formation occurs if the following force equation holds

$$F_d \geq F_\sigma + F_b, \quad (6)$$

where F_d , F_σ and F_b are the drag force, surface tension force and buoyancy, respectively. The forces in Eq. 6 are defined as

$$F_d = \frac{1}{2} \rho_s u_i^2 \frac{\pi}{4} d_D^2, \quad (7)$$

$$F_\sigma = \sigma \pi d_D, \quad (8)$$

$$F_b = \frac{1}{6} g (\rho_m - \rho_s) \pi d_D^3. \quad (9)$$

Now, the critical interfacial velocity, $u_{i,crit}$, i.e. the minimum velocity required for emulsification, for the droplet formation is obtained by substituting Eq. 7 - 9 into Eq. 6. The substitution yields

$$u_{i,crit} = \left(\frac{8\sigma}{\rho_s d_D} + \frac{4}{3} \frac{\rho_m - \rho_s}{\rho_s} g d_D \cos \alpha \right)^{1/2}. \quad (10)$$

Increasing d_D would cause the first term to approach zero and the latter term inside the parenthesis to approach infinity. On the other hand, decreasing d_D would push the first term to infinity and make the latter term vanish entirely. Thus, it can be deduced that the right hand side of Eq. 10 must have a minimum for some $d_{D,crit}$. The minimum is easily obtained by differentiation of Eq. 10 with respect to d_D and set equal to zero. Afterwhich $d_{D,crit}$ can be solved. The following equations are obtained for $d_{D,crit}$ and $u_{i,crit}$

$$d_{D,crit} = \left(\frac{6\sigma}{g(\rho_m - \rho_s) \cos \alpha} \right)^{1/2} \quad (11)$$

$$u_{i,crit} = \left(\frac{8}{\rho_s} \right)^{1/2} \left(\frac{2}{3} \sigma g (\rho_m - \rho_s) \cos \alpha \right)^{1/4}. \quad (12)$$

If $u_i > u_{i,crit}$ then Eq. 10 must be solved for the droplet diameter. Solving the equations yields

$$d_D = \frac{3}{8} \frac{\rho_s u_i^2}{g(\rho_m - \rho_s) \cos \alpha} \left(1 - \left(1 - \frac{128\sigma g (\rho_m - \rho_s) \cos \alpha}{3\rho_s^2 u_i^4} \right)^{1/2} \right). \quad (13)$$

In addition to the droplet size and critical velocity, equations for determining the interfacial velocity, u_i , and number of formed droplets per unit time, \dot{N} , have been derived. Due to the notable length, the equation for u_i is presented without the rigorous derivation. However, the derivation is based on boundary layer theory. It has to be remarked that some strong assumptions were made prior to the derivation. The equation for the interfacial velocity presented below cannot be solved analytically but requires a numerical solution. Furthermore, it was formulated for a dimensionless velocity $U = u_i/u_m$ at position $y = l$:

$$U = 0.1367 \left(\frac{\rho_m}{\rho_s} \right)^{2/3} \left(\frac{\rho_m l}{\nu_s} \right)^{1/3} \left(\frac{\rho_m l}{\nu_m} \right)^{-2/15} ((1-U)(0.1108 - 0.0693U))^{2/15}. \quad (14)$$

Here u_m is the velocity of the bulk steel and l is the length of the interface. Instead of u_m , the use of the mean value \bar{u}_m was suggested in Eq. 14. The mean value can be calculated using Eq. 15:

$$\bar{u}_m = u_{m,0} + \frac{2}{3} \left(2g \left(1 - \frac{\rho_s}{\rho_m} \right) l \cos \alpha \right)^{1/2}, \quad (15)$$

where $u_{m,0} = (2gh)^{1/2}$ and h is the plume height above the level of the slag surface. The birth rate of droplets, \dot{N} , is given by

$$\dot{N} = \frac{0.4153D\rho_s^{1/2}\mu_s^{1/2}l^{1/2}u_i^{5/2}}{d_D^2\sigma + \frac{1}{6}d_D^4g(\rho_m - \rho_s)\cos\alpha}. \quad (16)$$

The derivation of Eq. 16 is omitted as well; it is based on studying the kinetic energy on the slag side of the interface.

Wei & Oeters published a study [32] where the emulsification model was validated. The experiment was divided into two parts and two different modelling setups were used. In both setups cyclohexane and water were used to model slag and steel, respectively. The first part consisted of measurements in a gas-stirred system with the flow rate varying from 50 to 500 cm^3/s . The volume fraction of the cyclohexane was measured by taking probe samples. Samples of fixed total volume were taken from four locations at the same time to observe emulsification intensity. Only a qualitative analysis of the results from this part was reported. The second part concentrated on the actual droplet formation by comparing the results of the mathematical model and a water-oil model. It was noticed the mathematical model was able to predict the droplet formation rate very well. The average droplet diameter was calculated as function of water stream velocity at the oil-water interface. Comparison of the results proved that the predicted diameters were in good agreement with the experimental data with higher water stream velocities. With lower velocities the calculated diameters deviated more from the experimental data. The results are presented in Figs. 10 (a) and 10 (b).

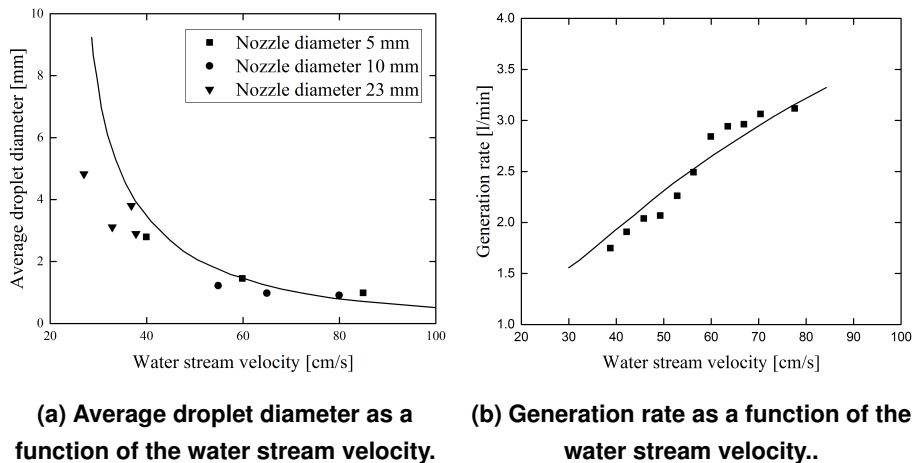


Fig. 10. Validation results of the Oeters' mathematical model. Figures were re-drawn from the figures of Wei and Oeters [32].

Senguttuvan et al.

Senguttuvan et al. [33] have developed a CFD model for studying slag emulsification in gas-stirred ladles. Their study considered the effect of gas flow rate, slag viscosity and

interfacial tension between slag and steel on the droplet formation. The model applied the Volume Of Fluid (VOF) method for tracking the interface between the slag and steel. For taking into account the effect of turbulence the VOF model was coupled with the Large Eddy Simulation (LES) method. They published two studies [33, 34]. The cases that were performed in their first study are presented in Table 3.

Table 3. The simulated cases in [33].

	ρ_S [kg/m ³]	ρ_L [kg/m ³]	μ_S [Pa s]	μ_L [Pa s]	σ [N/m]	u_{inlet} [m/s]
Oil-water						
Case 1	903	997	0.06134	0.00088	0.01304	0.236
Case 2	867	997	0.1498	0.00088	0.01295	0.317
Steel-slag						
Case 3	2650	6800	0.18	0.005	0.5	0.8
Case 4	2650	6800	0.18	0.005	1.0	0.8
Case 5	2800	7000	0.11	0.005	0.5	0.6
Case 6	2800	7000	0.22	0.005	0.5	0.6
Case 7	2800	7000	0.11	0.005	1.0	0.6

The CFD model in the first paper was constructed and validated based on the physical model experiments of Savolainen *et al.* [5]. For testing the validity of the model the work was carried out in two stages: 1) Modelling of the inlet half of the apparatus for determining the proper inlet velocity as a boundary condition for the actual emulsification model by solving Reynolds averaged Navier-Stokes (RANS) equations coupled with the Synthetic Eddy Method (SEM) and 2) Modelling of slag emulsification, i.e. the outlet side of the apparatus, by applying the Volume of Fluid (VOF) method and the Large Eddy Simulation (LES) method. The adopted approach is illustrated in Fig. 11. The obtained inlet velocity was applied in the test cases. Two cases of Savolainen *et al.* were simulated with the CFD model and the results were validated against the results from their physical model. In addition, simulations using slag and metal phases were conducted as in PAPER I. Other cases were modelled by using only the emulsification model and scaling the inlet velocity up or down.

The model of Senguttuvan *et al.* contained only two phases, slag and steel. The gas phase was excluded from the model. During the calculations a refinement of the mesh was employed in critical regions of the flow, i.e. from the inlet to the onset of

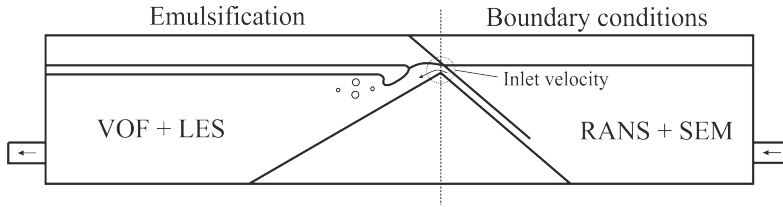


Fig. 11. Schematic figure of the computational domain. The right half of the domain was modelled using RANS and SEM methods and the left half where the emulsification occurs was modelled using VOF and LES methods. [33]

the emulsification. A grid size interval of 0.8-6.0 mm was reported. The tracking of the droplets was done in such a way that every droplet was counted only once and then removed from the domain. In this manner, the authors were able to calculate the emulsification rate and droplet size distribution. Thus, the possible break-up or coalescence of droplets was not observed in the model. In their first study, Senguttuvan *et al.* simulated two cases of Savolainen *et al.* using the model. They also simulated two slag-steel cases that were earlier simulated in PAPER I.

In their second study [34] different computational domains were utilized, see Fig. 12. The velocity boundary condition at the inlet was connected to the gas flow rate from the bottom plug of the ladle. The velocity boundary condition was determined from simulations of a full scale ladle. The simulated cases are presented in Table 4. In the simulations, the inlet size was set to the slag thickness. The effect of slag viscosity and interfacial tension on the droplet size is presented in Fig. 13 (a). Some of the cases were simulated with a constant slag thickness. In reality, a larger gas flow rate creates a larger open-eye and the slag is pushed towards the ladle wall which results in a greater slag layer thickness. This effect has been taken into account in the cases that are in the diagonal of the sub matrices in Table 4. The comparison between constant and varying slag thickness is presented in Fig 13 (b).

Table 4. The simulated cases in [34].

Q [lpm/ton]	2.0			4.0			6.0		
σ [N/m] \rightarrow	0.25	0.5	1.0	0.25	0.5	1.0	0.25	0.5	1.0
μ [Pa s] \downarrow									
0.005	x			x	x	x	x		
0.11		x		x	x	x		x	
0.22			x	x	x	x			x

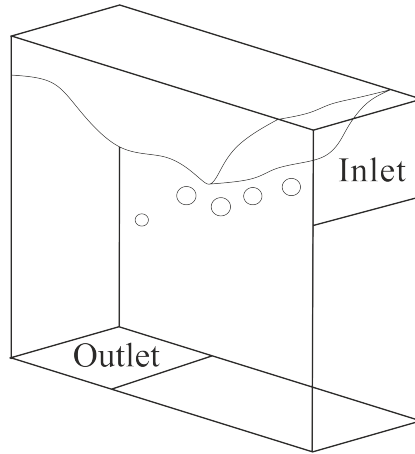


Fig. 12. Schematic figure of the computational domain utilized in the second study [34].

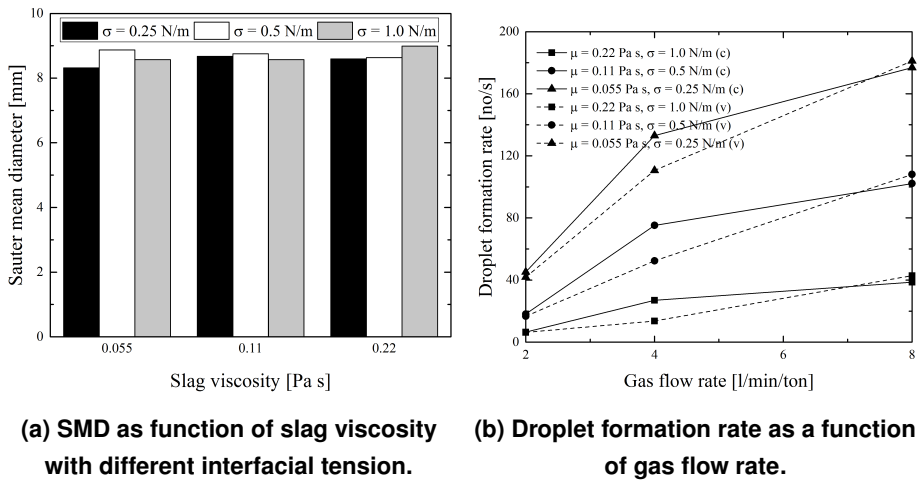


Fig. 13. Results from the simulations. Figures are re-drawn from the figures of Irons *et al.* [34].

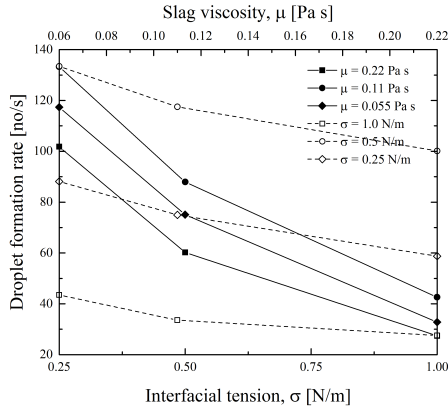


Fig. 14. Effect of slag viscosity (dashed line) and interfacial tension (solid line) on the droplet formation rate. The figure is re-drawn from the figure by Irons *et al.* [34].

Huang et al.

Huang *et al.* [35] combined CFD modelling and physical modelling (water-oil system) to study open-eye formation and slag droplet entrainment. It is a coupled VOF-LES model that is applied to model emulsified droplets. The droplets are tracked with a user defined function (UDF) code in the post-processing stage. Huang *et al.* stress the difficulty of the modelling phenomena, including such a small size scales as slag entrainment in a real scale ladle. The small ratio of slag droplets and the ladle dimensions induce a multiscale problem that it is computationally far too expensive to be modelled without restricting the examination to a smaller domain. Therefore, Huang *et al.* have developed an optimized model in which droplet formation is observed in a limited volume near the oil/slag-water/steel interface. The purpose of the study was to examine the effect of gas flow rate on the open-eye size and slag droplet formation.

Prior to actual CFD simulations, extensive analytical and experimental studies were carried out in order to determine suitable parameters for the CFD model. In the analytical part of the study the boundary conditions needed in the model were determined. The boundary conditions consisted of the inflow velocity of steel at different parts of the observed domain. The velocity distribution was assumed to follow a Gaussian distribution in the open eye region. It appeared that the boundary conditions are dependent on the following *critical parameters*: the velocity at the top of the gas plume, $u_{p,max}$ and the velocity distribution width parameter, n . The expression for the distribution width was taken from the literature. The velocity at the top of the plume was

determined experimentally by simulating a 300 t ladle with a 1:3 physical model with an eccentric bottom plug. By applying different gas flow rates from the bottom, the velocity was measured and a linear function was fitted to the data. The critical parameters are of the following form:

$$n = \sqrt{2}c(H + h_0) \quad (17)$$

$$u_{p,max} = 0.015Q_g + 21, \quad (18)$$

where $c = 0.0565Q_g^{0.15}$, Q_g is the gas flow rate from the bottom, H is the height of the ladle and h_0 is the vertical distance between the bottom plug and the virtual point source representing the imaginary apex of the conical plume, which was approximated to be equal to zero in the study. The necessary boundary conditions in the CFD model are the velocity of the approaching flow, u_r , backward flow velocity, u_b , the angle of the approaching flow, α_E , the height of the approaching flow, h_r , the height of the backward flow, h_b , and the radius of the open-eye (see Fig. 15). The boundary conditions are calculated using the critical parameters n and $u_{p,max}$. The detailed derivation of the boundary conditions is presented in [36].

The physical properties of water, oil and air are given in Table 5. The schematic presentation of the computational domain is presented in Fig. 15. As for the results, the droplet size distributions, the amount of droplets, average droplet sizes and the open-eye size were plotted against the flow rate.

Table 5. The physical properties. [35]

Parameters	Values
Density of water	996.36 kg/m ⁻³
Dynamic viscosity of water	8.94 × 10 ⁻⁴ Pa s
Density of oil	808.50 kg/m ⁻³
Dynamic viscosity of oil	2.21 × 10 ⁻³ Pa s
Interfacial tension, water-oil	28 × 10 ⁻³ N m ⁻¹
Surface tension of oil	24 × 10 ⁻³ N m ⁻¹
Density of air	1.205 kg/m ⁻³
Dynamic viscosity of air	1.81 × 10 ⁻⁵ Pa s

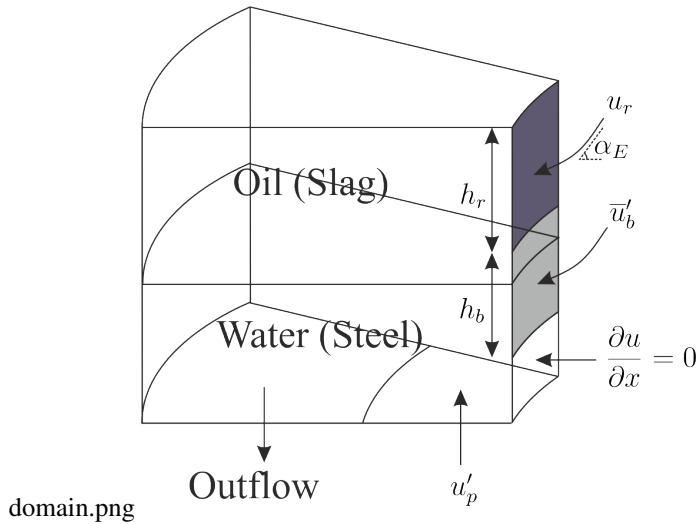


Fig. 15. Schematic of the computational domain with determined boundary conditions. The figure was re-drawn from the figure of Huang *et al.* [35].

The results of the model were validated against the measurements obtained from the water-oil system. Comparison of the calculated open-eye size and measured size as well as a comparison of modelled average droplet size and measured droplet size are presented in Fig. 16. The authors concluded that the analytical groundwork served well for determining the boundary conditions for the limited domain. It was reported that critical conditions for the emulsification were identified for certain cases. As for the droplet size, the authors concluded that the average droplet size increases with an increasing gas flow rate because the distribution broadens with higher flow rates. The dominant droplet size in the studied cases was 2-3 mm which corresponds to the results in PAPER I-III. From the physical model which was used to validate the results, slightly larger average droplet sizes compared to the simulations were detected, see Fig 16 (b). The author also reported good agreement between simulated open-eye size and measured open-eye size from the experiments, see Fig 16 (a).

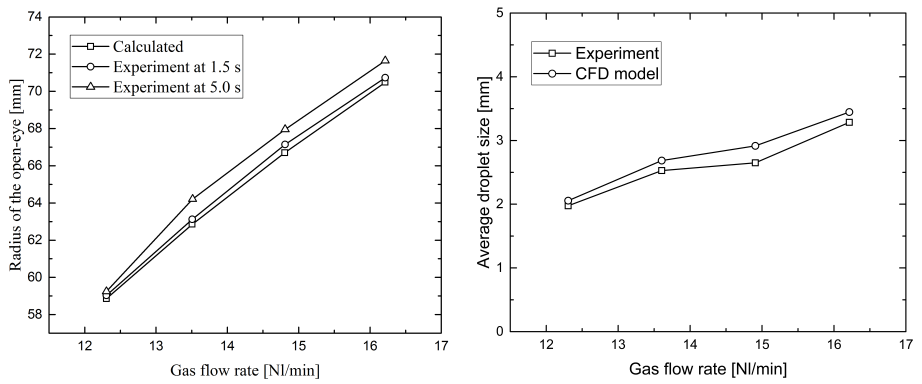


Fig. 16. Comparison between modelled open-eye size and measured open-eye size (a) and comparison between modelled average droplet size and measured droplet size (b). The figures were re-drawn from the figures of Huang *et al.* [35].

4 Description of the models

Developing a phenomena based model for a complex process stage involving high temperatures requires the description of many physical and thermodynamic properties. In modelling chemical reactions and heat transfer during slag reduction, determining slag droplet area, mass transfer coefficients, activities of the species and heat transfer coefficients have the most important role. In this chapter, the applied submodels and descriptions are introduced.

4.1 Modelling of emulsification of slag

Emulsification of slag, i.e. the generation of slag droplets, during bottom blowing was studied by means of Computational Fluid Dynamics (CFD) simulations. Emulsification studies using a water-oil model carried out by Savolainen *et al.* [5] formed the basis for the simulations. The geometry in the CFD simulations was constructed based on the apparatus used in their physical modelling. The computational domain is presented in Fig. 17. The preliminary CFD simulations regarding emulsification also rested on the cases studied in their work (PAPER I). The dimensions of the domain were 30 cm in the z-direction and 10 cm in the y- and z-direction.

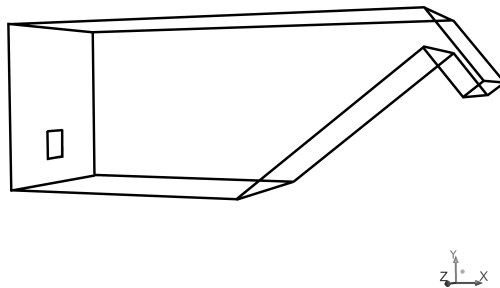


Fig. 17. Computational domain for simulating the emulsification of slag.

The CFD simulations were carried out as 3-dimensional, three phase simulations, including slag, steel and gas phases. In order to identify generated slag droplets, it was essential to track the interface between the slag and steel. For this purpose, the Volume

Of Fluid (VOF) method was applied. The Large Eddy Simulation (LES) method was chosen for modelling turbulence. In the following, the applied models are introduced in more detail. The results from the CFD model were employed to implement an emulsification module to the reduction stage model.

The reason for simulating the emulsification in a small domain instead of a real size ladle was due to the fact that slag droplets are quite small, typically only a couple of millimeters in size. Thus, it would have been computationally very expensive to simulate formation of such small droplets in a full scale system.

The CFD simulations were carried out using ANSYS Fluent software. All simulations were carried out with an explicit VOF method coupled with an LES turbulence model. The size of the time-step was determined so that the global Courant number was always smaller than 1. The following boundary conditions were applied: a) Velocity inlet (the given velocity at the inlet) b) Outflow outlet (volume outflow = volume inflow) and c) No-slip boundary condition at the domain walls.

4.1.1 The Volume Of Fluid method (VOF)

The Volume Of Fluid method is a numerical method for tracking fluid-fluid interfaces. The method was developed in the 1970s and belongs to the class of *Eulerian methods* in which fluid flow is observed in a fixed coordinate system (i.e. in the laboratory frame of reference).

The VOF method is based on a volume fraction function that is defined for every fluid present in the calculation in each computational cell. If the volume fraction of fluid or phase i is denoted by C_i , three possible conditions are possible in a computational cell: 1) $C_i = 0$, i.e. the phase is not contained in the cell, 2) $C_i = 1$, i.e. the cell is fully occupied by the phase and $0 < C_i < 1$, the cell contains an interface between phase i and one or more other phases. The conservation equation for the volume fraction in the case of an incompressible flow is written as follows:

$$\frac{\partial C_i}{\partial t} + \mathbf{u} \cdot \nabla C_i = 0 \quad (19)$$

Regarding material properties that appear in transport equations, e.g. densities and viscosities, only one such property is defined in each computational cell. The properties are calculated in terms of volume fractions and properties of individual phases to obtain one value in each cell. For example, the density is calculated in the following manner:

$$\rho = \sum_i C_i \rho_i, \quad (20)$$

where ρ_i is the density of phase i .

In the VOF method only one momentum equation is solved and the resulting field is shared by all phases. The momentum equation depends on the volume fractions through material properties. The momentum equation is defined as:

$$\frac{\partial \mathbf{u}}{\partial t} + \nabla \cdot (\mathbf{u} \otimes \mathbf{u}) = -\nabla p + \nu \nabla^2 \mathbf{u} + \mathbf{g} + \frac{1}{\rho} \mathbf{F}, \quad (21)$$

where \mathbf{u} is the velocity, ν is the kinematic viscosity, p is the pressure, \mathbf{g} is the force due to gravity and \mathbf{F} is the volume force that takes into account the effects of surface tension between phases. \mathbf{F} is modelled using the Continuum Surface Force (CSF) [37] model as follows:

$$\mathbf{F} = \sum_i \sum_{j, i < j} \sigma_{ij} \frac{C_i \rho_i \theta_j \nabla C_j + C_j \rho_j \theta_i \nabla C_i}{\frac{1}{2} (\rho_i + \rho_j)}. \quad (22)$$

In Eq. 22, the curvature θ_i is defined as:

$$\theta_i = \frac{\nabla^2 C_i}{|\nabla C_i|}, \quad (23)$$

where ∇^2 is the Laplace operator.

In the VOF method, the procedure is to first solve the velocity field and after that update the volume fractions [38]. In order to solve the velocity field, the conservation equation of momentum has to be coupled with the conservation equation of mass. In the following section we will consider the governing equations for incompressible turbulent flow coupled with a suitable turbulence model.

4.1.2 The Large Eddy Simulation model (LES)

The formation of eddies of different length scales is characteristic in turbulent flows. In principle, direct resolving each length scale is possible. This method is called Direct Numerical Simulation (DNS). However, this approach is very demanding in terms of computational cost. Therefore, in order to take turbulence into account without unreasonably increasing the calculation time, the use of a suitable turbulence model was needed. In this work, it was decided to apply the Large Eddy Simulation model. A

number of textbooks have been published concerning the LES modelling. In this section a brief introduction to LES in the case of incompressible fluid flow is provided. Another choice for modelling the turbulence would have been the use of the Reynold Averaged Navier-Stokes (RANS) equations. This approach is even faster computationally than the LES approach. However, the RANS equations are time-averaged for all turbulent scales and, therefore, it was assumed that a more realistic result would be reached using an approach which lies somewhere between the DNS approach and using the RANS equations.

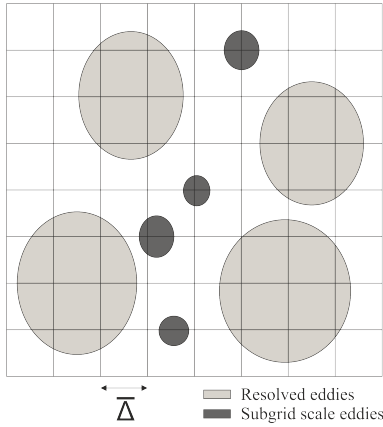
The LES model is based on the idea that eddies larger than a certain scale are resolved directly and smaller scales are modelled. The resolved length scales are reduced by applying *low-pass filtering*. The filtering removes the small scale, i.e. the sub-grid scale, information from the numerical solution. The sub-grid scale means that length scales that are smaller than the grid size are filtered out. However, these scales cannot just be omitted since they have great influence on the flow behavior. Most of the kinetic energy is contained in the large scale structures and energy is transferred between scales. The instability of the flow causes large structures to break into smaller and smaller eddies. Eventually, the eddies become small enough and their kinetic energy is dissipated into heat by viscous effects. This process is called *energy cascade*. Turbulence is a multiscale phenomenon by nature, i.e. interactions between very different scales occur, which means that neglecting scales is not possible without falsifying the dynamics of all scales [39]. The schematical presentation of the energy cascade in the wave number space is presented in Fig. 18b. As it can be seen most of the energy is contained at low wave numbers. The energy spectrum decreases as the wave number increases. In the LES approach, a cut-off length, κ_c , is applied for separating the resolved scales from the scales that are modelled.

The fluid motion for the incompressible fluid is governed by the equation for the conservation of mass (Eq.24) (i.e. the continuity equation) and the equation for the conservation of momentum (Eq.25):

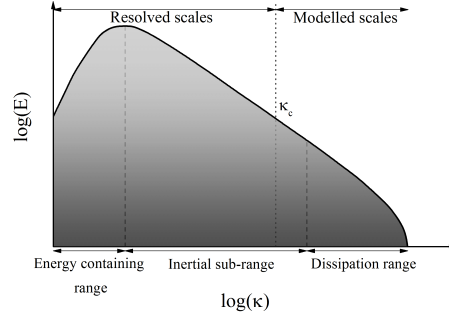
$$\nabla \cdot \mathbf{u} = 0 \quad (24)$$

$$\frac{\partial \mathbf{u}}{\partial t} + \nabla \cdot (\mathbf{u} \otimes \mathbf{u}) = -\nabla p + \nu \nabla^2 \mathbf{u}. \quad (25)$$

To be exact, the form of the momentum conservation in our case is as in Eq. 21. However, for the sake of simplicity we do not carry the gravitational force term, \mathbf{g} , and surface tension force term, $\frac{1}{\rho} \mathbf{F}$, in this section. These terms remain the same despite of



(a) Eddies in physical space [39].



(b) Typical shape of the energy spectrum in Fourier space [39, 40].

Fig. 18. Representation of different eddy scales in physical space and Fourier space.

the scale separation procedure applied to the equations and they can be added into the equations as such after the filtering has been done.

The low-pass filtering in LES is defined as a convolution product. The following equation formally gives the definition for the resolved part \bar{f} of the variable f

$$\bar{f}(\mathbf{x}, t) = \int f(\mathbf{y}, t) G(\mathbf{x} - \mathbf{y}) d\mathbf{y} \quad (26)$$

The sub-grid part of the flow field, which is usually denoted by f' , is obtained from Eq. 27

$$f = \bar{f} + f'. \quad (27)$$

The filtered continuity equation and the momentum equation are, respectively, as follows

$$\nabla \cdot \bar{\mathbf{u}} = 0 \quad (28)$$

$$\frac{\partial \bar{\mathbf{u}}}{\partial t} + \nabla \cdot (\overline{\mathbf{u} \otimes \mathbf{u}}) = -\nabla \bar{p} + \nu \nabla^2 \bar{\mathbf{u}}. \quad (29)$$

The filtering process produces a non-linear term $\overline{\mathbf{u} \otimes \mathbf{u}}$. In order for Eq. 29 to be usable, the non-linear term has to be expressed in terms of $\bar{\mathbf{u}}$ and \mathbf{u}' .

If the decomposition according to Eq. 27 is substituted to Eq. 29 we have

$$\frac{\partial \bar{\mathbf{u}}}{\partial t} + \nabla \cdot (\overline{\mathbf{u} \otimes \mathbf{u}}) = -\nabla \bar{p} + \nu \nabla^2 \bar{\mathbf{u}} - \nabla \cdot \boldsymbol{\tau}_{SGS}. \quad (30)$$

In Eq. 30 term $\boldsymbol{\tau}_{SGS}$ is the sub-grid stress tensor which is written as

$$\boldsymbol{\tau}_{SGS} = \overline{\mathbf{u} \otimes \mathbf{u}} - \overline{\bar{\mathbf{u}} \otimes \bar{\mathbf{u}}} = \underbrace{\overline{\mathbf{u} \otimes \mathbf{u}'} + \overline{\mathbf{u}' \otimes \bar{\mathbf{u}}}}_{\mathbf{C}} + \underbrace{\overline{\mathbf{u}' \otimes \mathbf{u}'}}_{\mathbf{R}}. \quad (31)$$

The term \mathbf{C} is the cross stress tensor which represents the interactions between large scales and small scales. \mathbf{R} is the Reynolds subgrid stress tensor which characterizes the effect of small scales on the flow.

Since the term $\overline{\mathbf{u} \otimes \bar{\mathbf{u}}}$ can not be calculated directly, another decomposition according to Eq. 32 is introduced:

$$\overline{\mathbf{u} \otimes \bar{\mathbf{u}}} = \underbrace{(\overline{\mathbf{u} \otimes \bar{\mathbf{u}}} - \bar{\mathbf{u}} \otimes \bar{\mathbf{u}})}_{\mathbf{L}} + \bar{\mathbf{u}} \otimes \bar{\mathbf{u}} \quad (32)$$

Subsequently, we obtain the final form of the filtered momentum equation:

$$\frac{\rho \bar{\mathbf{u}}}{\partial t} + \nabla \cdot (\overline{\mathbf{u} \otimes \bar{\mathbf{u}}}) = -\nabla \bar{p} + \nu \nabla^2 \bar{\mathbf{u}} - \nabla \cdot \boldsymbol{\tau}_{SGS}, \quad (33)$$

where the subgrid tensor is as follows

$$\boldsymbol{\tau}_{SGS} = \mathbf{L} + \mathbf{C} + \mathbf{R}. \quad (34)$$

In addition to \mathbf{C} and \mathbf{R} , the term \mathbf{L} , which is known as the Leonard tensor, describes the interactions among the large scales. The decomposition presented in Eq. 34 is called the Leonard decomposition or triple composition [39, 40].

According to Sagaut [40], scale separation is essentially done for reducing the number of degrees of freedom of the solution. Consequently, the information on the small scales, represented by \mathbf{u}' , is lost. All this information is contained in the subgrid scale tensor $\boldsymbol{\tau}_{SGS}$. To consider the correct dynamics of the resolved scales, however, the small scales have to be somehow taken into account. In other words, $\boldsymbol{\tau}_{SGS}$ has to be modelled. The modelling consists of approximating $\boldsymbol{\tau}_{SGS}$ in terms of the resolved scales. Plenty of different models for $\boldsymbol{\tau}_{SGS}$ exist in the literature, even different modelling strategies for the problem are provided. Going into detail of the models and modelling strategies are beyond the scope of this work. In this work the subgrid tensor is modelled

by employing the Boussinesq hypothesis. The modelled tensor, written with index notation, is as follows:

$$\tau_{ij}^{SGS} = 2\nu_{SGS}\bar{S}_{ij} + \frac{1}{3}\tau_{kk}\delta_{ij}, \quad (35)$$

where δ_{ij} is the Kronecker delta and \bar{S}_{ij} is the rate of strain tensor which is defined as

$$\bar{S}_{ij} = \frac{1}{2} \left(\frac{\partial \bar{u}_i}{\partial x_j} + \frac{\partial \bar{u}_j}{\partial x_i} \right). \quad (36)$$

The above formulation introduces another variable, subgrid viscosity or turbulent viscosity ν_{SGS} . This variable has to be modelled as well. As with the subgrid scale tensor, there are number of methods for modelling subgrid viscosity. Models for ν_{SGS} can be divided in to three classes: 1) Models based on resolved scales, 2) models based on the energy at the cut-off, $E(\kappa_c)$, and 3) models based on subgrid scales. In this work the Smagorinsky-Lilly model was applied for modelling ν_{SGS} . The Smagorinsky-Lilly model belongs to class 1) and it is, thus, based on the resolved scales [40]. The Smagorinsky-Lilly model is given by Eq. 37:

$$\nu_{SGS} = L^2 \sqrt{2\bar{S}_{ij}\bar{S}_{ij}}, \quad (37)$$

where $L = \min(\xi d, C_s \bar{\Delta})$. In the expression of variable L , ξ , d , C_s and $\bar{\Delta}$ are the von Kármán constant (which is typically denoted by κ but here we use ξ to avoid confusion with the wave numbers), the distance from the nearest wall, the Smagorinsky constant and cut-off length associated with the filter, respectively. In practice, the ANSYS Fluent defines the filter width as

$$\bar{\Delta} = V^{\frac{1}{3}}, \quad (38)$$

where V is the volume of the computational cell. As for the constants, $\xi = 0.4$ and $C_s = 0.1$. The second term in Eq. 35 is added to the filtered static pressure field, \bar{p} , and does not require modelling. This yields:

$$\bar{P} = \bar{p} + \frac{1}{3}\tau_{kk}. \quad (39)$$

Finally, we have obtained a set of filtered conservation equations for the turbulent incompressible flow in closed form that can be solved as follows:

$$\nabla \cdot \bar{\mathbf{u}} = 0 \quad (40)$$

$$\frac{\partial \bar{\mathbf{u}}}{\partial t} + \nabla \cdot (\bar{\mathbf{u}} \otimes \bar{\mathbf{u}}) = -\nabla \bar{P} + (\nu + \nu_t) \nabla^2 \bar{\mathbf{u}}. \quad (41)$$

4.2 The slag reduction model of the CAS-OB process

The slag reduction model is a phenomena based model for solving chemical reactions and heat transfer during the reduction stage in a time-dependent manner. The model consists of several modules and submodels that are needed for describing mass transfer, heat transfer, the interfacial area between the slag and steel, activities of the species etc.

The flow chart of the model code is presented in Fig. 19. In the first stage the initial data and geometry data is read. The second stage is the update stage in which the operational data, compositions and temperatures, as well as interfacial area, are updated at beginning of new time step. This stage is followed by the actual computational modules. The chemical reaction system is solved in the third stage and the heat transfer is solved in the subsequent stage. In practise, the modules for modelling reactions and heat transfer are iterative calculation loops for solving systems of partial differential equations. The equations that are introduced later in this Chapter describe the conservation of the mass of the species in slag, steel and gas, as well as the conservation of the total mass of the phases and conservation of heat.

As it can be seen from Fig. 38, the model is constructed so that the reactions and heat transfer are solved separately. Attempts at simultaneously solving both systems has proved to lead severe instabilities in the model, although, in principle, it should be possible. However, a similar approach has been applied in other models and the error caused by this procedure when using small time steps is quite small [41–43]. A simultaneous solution is certainly desirable in the future.

In the following Sections, we will proceed to define the reaction system in the slag reduction of the CAS-OB process. Subsequently, the governing equations for the mass and heat transfer are given. Finally, the submodels applied in the slag reduction model are introduced.

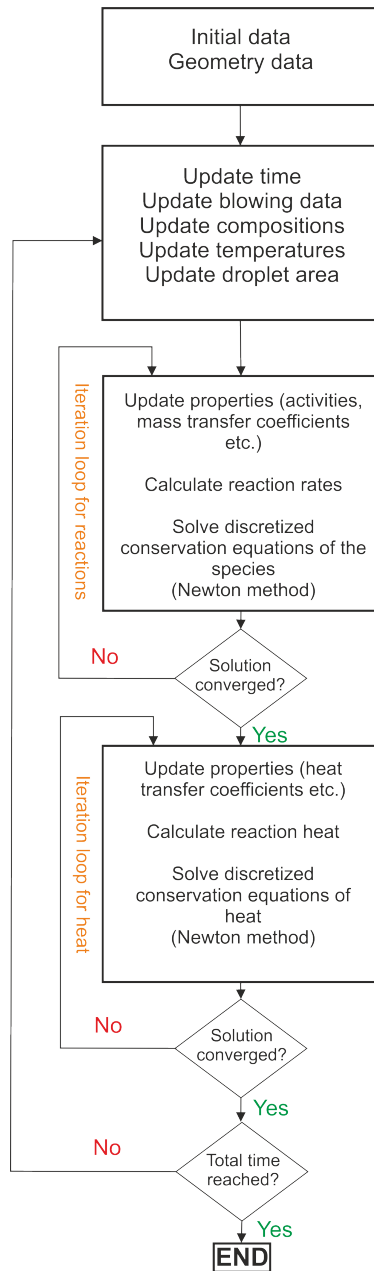
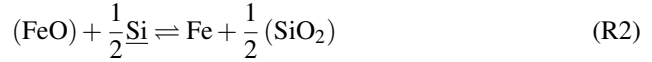
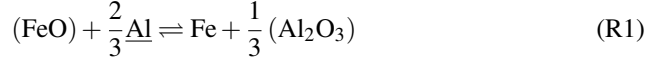


Fig. 19. Flow chart of the reduction stage model.

4.2.1 The reaction system and the governing equations in the model

The reaction system

In the present model the steel phase is an Fe-Ni-Al-Si-Mn-C alloy. The slag phase consists of Al_2O_3 , SiO_2 , MnO , CaO and FeO . The system of reactions examined in the model are as follows:



The reaction rates corresponding to reactions R1-R4 were formulated according to the modified law of mass action method. The reaction rate equations are given by:

$$R_1 = k_{f_1} \left(a_{\text{FeO}} a_{\underline{\text{Al}}}^{2/3} - \frac{a_{\text{Fe}} a_{\text{Al}_2\text{O}_3}^{1/3}}{K_1} \right) \quad (42)$$

$$R_2 = k_{f_2} \left(a_{\text{FeO}} a_{\underline{\text{Si}}}^{1/2} - \frac{a_{\text{Fe}} a_{\text{SiO}_2}^{1/2}}{K_2} \right) \quad (43)$$

$$R_3 = k_{f_3} \left(a_{\text{FeO}} a_{\underline{\text{Mn}}} - \frac{a_{\text{Fe}} a_{\text{MnO}}}{K_3} \right) \quad (44)$$

$$R_4 = k_{f_4} \left(a_{\text{FeO}} a_{\underline{\text{C}}} - \frac{a_{\text{Fe}} a_{\text{CO}}}{K_4} \right) \quad (45)$$

$$(46)$$

Due to the fact that the reactions observed here take place at high temperatures, approximately 1600 °C, and, thus, are extremely fast, it has been assumed that the reactions are controlled by mass transfer rather than reaction kinetics. It has been proven that under such conditions, if the forward reaction rate coefficient, k_f , approaches infinity, mass transfer limited equilibrium will be reached at the reaction interface [41]. Computationally, it is not possible to set infinite values for k_f but with sufficiently high values the equilibrium can be obtained with acceptable accuracy. A dimensionless

property, *the equilibrium number E*, was applied to confirm that the system approaches equilibrium. By allowing a small deviation of *E* from zero (< 0.1%) in the calculations, it was ensured that the equilibrium at the interface was reached. The equilibrium number condition for reaction *i* is formulated as follows:

$$E_i = \left| 1 - \frac{Q_i}{K_i} \right| < 0.001, \quad (47)$$

where Q_i is *the reaction quotient* defined by:

$$Q_i = \frac{\prod_{p_i} a_{p_i}^{v_{p_i}}}{\prod_{r_i} a_{r_i}^{v_{r_i}}}. \quad (48)$$

I.e. the reaction quotient is the quotient of the product of the reaction product activities, a_{p_i} , of reaction *i* raised to the power of the corresponding stoichiometric coefficient v_{p_i} and similar product of the reactant activities.

The conservation of the species

To define the conservation of mass within the observed system, a conservation equation for every species in the bulk phase and at the interface as well as a conservation equation of the total mass for every phase is needed. The conservation equations are presented in the discretized form here. The conservation of species *i* in the bulk phase is formulated as follows:

$$\frac{m_L^t y_{L,i}^t - m_L^{t-1} y_{L,i}^{t-1}}{\Delta t} = -A_\varepsilon h_L \rho_L (y_{i,L} - y_{i,\varepsilon}) \quad (49)$$

$$\frac{m_S^t y_{S,i}^t - m_S^{t-1} y_{S,i}^{t-1}}{\Delta t} = -A_\varepsilon h_S \rho_S (y_{i,S} - y_{i,\varepsilon}) \quad (50)$$

$$\frac{m_G^t y_{G,i}^t - m_G^{t-1} y_{G,i}^{t-1}}{\Delta t} = -A_\varepsilon h_G \rho_G (y_{i,G} - y_{i,\varepsilon}) \quad (51)$$

In Eq. 49-51 m_L , m_S and m_G are the mass of liquid steel, slag and gas, respectively, $y_{L,i}$, $y_{S,i}$ and $y_{G,i}$ refer to species *i* in steel, slag and gas, respectively, A_ε is the area of the interface (i.e. the are of the slag droplets), *t* is time, ρ is density and h_L , h_S and h_G are the mass transfer coefficients in steel, slag and gas.

The conservation of the total mass of the bulk phases is obtained by summing Eq. 49-51 over all species:

$$\frac{m_L^t - m_L^{t-1}}{\Delta t} = -A_\varepsilon \sum_{i=1}^{N_s} \Gamma_{L,i} h_L \rho_L (y_{i,L} - y_{i,\varepsilon}) \quad (52)$$

$$\frac{m_S^t - m_S^{t-1}}{\Delta t} = -A_\varepsilon \sum_{i=1}^{N_s} \Gamma_{S,i} h_S \rho_S (y_{i,S} - y_{i,\varepsilon}) \quad (53)$$

$$\frac{m_G^t - m_G^{t-1}}{\Delta t} = -A_\varepsilon \sum_{i=1}^{N_s} \Gamma_{G,i} h_G \rho_G (y_{i,G} - y_{i,\varepsilon}). \quad (54)$$

Above, in Eq. 52-54, N_s is the number of all species and $\Gamma_{L,i}$, $\Gamma_{S,i}$ and $\Gamma_{G,i}$ are binary variables that equal to one if species i is in a denoted phase and zero otherwise.

As for the interface, it has to be noted that the interface is assumed to be massless. It follows that there is no storage of the species, i.e. the derivative of mass with respect to time is zero. The conservation of mass at the interface is formulated as follows:

$$h_L \rho_L (y_{i,L} - y_{i,\varepsilon}) + \sum_{j=1}^{N_r} \tilde{v}_{i,k} R_k = 0 \quad (55)$$

$$h_S \rho_S (y_{i,S} - y_{i,\varepsilon}) + \sum_{j=1}^{N_r} \tilde{v}_{i,k} R_k = 0 \quad (56)$$

$$h_G \rho_G (y_{i,G} - y_{i,\varepsilon}) + \sum_{j=1}^{N_r} \tilde{v}_{i,k} R_k = 0. \quad (57)$$

In Eq. 55-57, N_r is the number of reactions and $\tilde{v}_{i,k}$ is the mass-based stoichiometric coefficient which is defined as:

$$\tilde{v}_{i,k} = v_{i,k} \frac{M_i}{M_{k,K}}, \quad (58)$$

where $v_{i,k}$ is the stoichiometric coefficient, M_i is the molar mass of species i and $M_{k,K}$ is the molar mass of key component, K , of reaction k .

The conservation of heat

In the reduction model, the conservation of heat is considered in the bulk phases, in the ladle walls and at the reaction interface. The conservation equations in the steel, slag and gas phases are as follows:

$$\begin{aligned}
\frac{c_{p,L}m_L(T_L^n - T_L^{n-1})}{\Delta t} &= \dot{m}_{Ar}c_{p,Ar}(T_L - T_{Ar,in}) - \alpha_L A_\varepsilon (T_L - T_\varepsilon) \\
&\quad - \alpha_{L_{in}} A_{L_{in}} (T_L - T_{L_1}) - \varepsilon_L \sigma A_O (T_L^4 - T_{Atm}^4) \\
&\quad - A_\varepsilon (T_L - T_\varepsilon) \sum_{i=1}^{N_s} \sum_{j=1}^{N_r} \Gamma_{L,i} R_j \tilde{v}_{i,j} c_{p,i}
\end{aligned} \tag{59}$$

$$\begin{aligned}
\frac{c_{p,S}m_S(T_S^n - T_S^{n-1})}{\Delta t} &= -\alpha_S A_\varepsilon (T_S - T_\varepsilon) \\
&\quad - A_\varepsilon (T_S - T_\varepsilon) \sum_{i=1}^{N_s} \sum_{j=1}^{N_r} \Gamma_{S,i} R_j \tilde{v}_{i,j} c_{p,i}
\end{aligned} \tag{60}$$

$$\begin{aligned}
\frac{c_{p,G}m_S(T_G^n - T_G^{n-1})}{\Delta t} &= -\alpha_G A_\varepsilon (T_G - T_\varepsilon) \\
&\quad - A_\varepsilon (T_G - T_\varepsilon) \sum_{i=1}^{N_s} \sum_{j=1}^{N_r} \Gamma_{G,i} R_j \tilde{v}_{i,j} c_{p,i}.
\end{aligned} \tag{61}$$

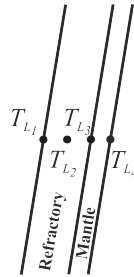
In the above, α_L , α_S , α_G and $\alpha_{L_{in}}$ are the heat transfer coefficients in steel, slag, gas and inner surface of the ladle, respectively. The heat capacity of steel, slag, gas and species i are denoted by $c_{p,L}$, $c_{p,S}$, $c_{p,G}$, $c_{p,Ar}$ and $c_{p,i}$, respectively. More detailed interpretation of the terms in Eq. 59-61 are given in PAPER IV.

The conservation of heat at the interface given by Eq. 62:

$$\alpha_L A_\varepsilon (T_L - T_\varepsilon) + \alpha_S A_\varepsilon (T_S - T_\varepsilon) + \alpha_G A_\varepsilon (T_G - T_\varepsilon) = \sum_{i=1}^{N_r} R_i \Delta h_i. \tag{62}$$

As for the heat transfer through the ladle walls, three additional equations are required. The ladle wall consists of the refractory lining and steel shell surrounding the lining. Temperatures are calculated at four points:

- 1) At the inner surface of the lining (T_{L_1})
- 2) In the middle of the lining (T_{L_2})
- 3) At the inner surface of the mantle (T_{L_3})
- 4) At the outer surface of the mantle (T_{L_4})



The equations are as follows:

$$\alpha_{L_{in}}(T_L - T_{L_1}) = \frac{k_R(T_{L_1} - T_{L_2})}{\frac{1}{2}\Delta x_R} \quad (63)$$

$$\frac{k_R A_{L_{in}}(T_{L_1} - T_{L_2})}{\frac{1}{2}\Delta x_R} = \frac{k_R A_M(T_{L_2} - T_{L_3})}{\frac{1}{2}\Delta x_R} + \frac{c_{p,R} m_R (T_{L_2}^n - T_{L_2}^{n-1})}{\Delta t} \quad (64)$$

$$\frac{k_R(T_{L_2} - T_{L_3})}{\frac{1}{2}\Delta x_R} = \frac{k_M(T_{L_3} - T_{L_4})}{\Delta x_M}. \quad (65)$$

4.2.2 The emulsification module for the reduction stage model of the CAS-OB process

Since the emulsification of slag increases the interfacial area between the slag and steel and, thus, has a great effect on the mass transfer between the phases, a quantitative submodel describing the emulsification was needed for the reduction stage model. From the CFD simulations we obtained the size distributions of the slag droplets (PAPER I-III). The distributions were studied by varying the physical properties of the phases and the flow velocity of the steel. Into the obtained data we fitted Rosin-Rammler-Sperling distribution functions. The RRS functions are of the following form:

$$R = 100 \exp\left(\frac{d}{d'}\right)^n. \quad (66)$$

Koria and Lange [44] have derived an equation based on Eq. 66 that relates the distribution to a limiting diameter, d_{lim} , which corresponds to $R = 0.001$. The function is as follows:

$$RF = 0.001 \left(\frac{d}{d_{lim}}\right)^n, \quad (67)$$

where n is a parameter that defines the shape of the distribution. The term d_{lim} was determined based on the simulation data after which n was determined by the least squares method. The obtained shape parameter was $n = 2.06 - 2.46$.

According to the fitted function we were able to determine the average size of the droplets. The emulsification module was constructed by combining the droplet size model and the formation rate model derived by Oeters [6]. By applying these models the interfacial area per unit time was determined. The equation for the formation rate is Eq. 16 presented in Section 4.1. The model for the formation rate requires determining

the interfacial velocity, u_i , at the interface between the slag and steel. The interfacial velocity can be obtained by solving Eqs. 14-15.

Another property appearing in Eq. 16 that must be determined is the diameter of the slag free area, i.e. the diameter of the open-eye, denoted by D . Krishnapisharody *et al.* developed a model for quantifying the area of the open-eye. They developed separate models for thick [45] and thin [12, 46] slag layers. In our model, since the slag thickness in the CAS-OB process is typically around 0.1 m, we apply the correlation for the thin slag layer. Their model describes the area as a function of bath height, slag layer height, density ratio of the slag and steel. All these quantities are available directly or can be calculated from the known properties. Assuming that the open-eye is circular, the diameter can be calculated easily from the area. The correlation for the dimensionless open-eye area is as follows [12]:

$$A_e^* = -0.76(Q^*)^{0.4} + 7.15(1 - \rho^*)^{-0.5} (Q^*)^{0.73} (h^*)^{-0.5}. \quad (68)$$

The parameters in Eq. 68 are given by

$$A_e^* = \frac{A_e}{H^2} \quad (69)$$

$$Q^* = \frac{Q}{g^{0.5} H^{2.5}} \quad (70)$$

$$\rho^* = \frac{\rho_S}{\rho_L} \quad (71)$$

$$h^* = \frac{h}{H}, \quad (72)$$

where A_e is the dimensional area, Q is the gas flow rate, H is the height of the bath, ρ_S is density of slag, ρ_L is density of steel and h is the height of the slag layer and g is the gravitational acceleration. In the derivation of the model, the ladle diameter is taken into account as well, but with some scaling analysis and averaging the correlation is simplified in such a way that the diameter of the ladle does not appear in the final equation.

The residence time of the droplets ultimately determines the magnitude of the area formed by the slag droplets. In the reduction model, only one average residence time, τ , was applied. According to Oeters [6], the residence time of slag droplets in a ladle is typically less than 60 seconds. Lacking any quantitative method for determining residence time, it was treated as an adjustment parameter. Bearing in mind the rule of thumb given by Oeters, the value of $\tau = 45$ s was utilized in the model.

4.2.3 The activity of the species

As it can be seen from Eq. 42-45, the reaction rates were formulated in terms of activities of the species and equilibrium constants. The thermodynamic definition of equilibrium constant is:

$$K = \exp\left(-\frac{\Delta G^\circ}{RT}\right), \quad (73)$$

where ΔG is the change of Gibbs free energy of the reaction, R is the universal gas constant and T is the temperature. By definition, the change of Gibbs free energy can be expressed as follows:

$$\Delta G^\circ = \Delta H^\circ - T\Delta S^\circ, \quad (74)$$

where ΔH° and ΔS° are the reaction enthalpy and reaction entropy, respectively. The values that have been applied for ΔH° and ΔS° in the model are presented in PAPER IV.

The Raoultian activity of species i is defined as

$$a_i = \gamma_i x_i, \quad (75)$$

where γ_i is the Raoultian activity coefficient and x_i is the mole fraction. In this model, the conservation equations of the species are formulated in terms of mass fraction and, thus, the activities need to be formulated in terms of mass fractions as well:

$$a_i = \gamma_i \frac{M_P}{M_i} y_i, \quad (76)$$

where M_i , M_P and y_i are the molar mass of species i , molar mass of phase containing species i and mass fraction of species i , respectively.

For modelling the activity coefficients γ_i , we chose to apply unified interaction parameter (UIP) formalism for the steel species [17] and Ban-Ya model [18] for slag species. According to UIP formalism, the activity coefficient is modelled according to Eq. 77-78:

$$\ln \gamma_i = \ln \gamma_{Fe} + \ln \gamma_i^\circ + \sum_j \frac{\varepsilon_i^j M_L}{M_j} \quad (77)$$

$$\ln \gamma_{Fe} = -\frac{1}{2} \sum_j \sum_k \frac{\varepsilon_j^k M_L^2}{M_j M_k}. \quad (78)$$

In the above equations, summations are taken over all steel species. The Raoultian activity coefficients in the infinite dilution, γ_i° , and first order binary interaction parameters, ϵ_k^j , were taken from the literature [47, 48]. The applied values are presented in PAPER IV.

The Ban-Ya model is a quadratic formalism that is based on the regular solution model [49]. According to Ban-Ya the Raoultian activity coefficient for species i is formulated as:

$$RT \ln \gamma_i = \sum_{\substack{j \\ j \neq i}} \alpha_{ij} X_j^2 + \sum_j \sum_{\substack{k=j+1 \\ j, k \neq i}} (\alpha_{ij} + \alpha_{ik} - \alpha_{jk}) X_j X_k + \Delta G_{conv}. \quad (79)$$

In Eq. 79, X_i is the cation fraction, α_{ij} is the interaction energy and ΔG_{conv} is the conversion factor between the regular solution and the real solution which is determined based on the chosen standard state, i.e. the Raoult standard state in our case. The cation fraction is defined as follows [50]:

$$X_i = \frac{y_i N_{O,i}}{M_i} \left(\sum_j \frac{y_j N_{O,j}}{M_j} \right)^{-1}. \quad (80)$$

In Eq. 80, $N_{O,i}$ is the number of O-atoms in species i . The conversion energies and interaction energies required in Eq. 79 were collected from the literature [51, 52]. The applied values are tabulated in PAPER IV.

4.2.4 Mass and heat transfer coefficients

In addition to the interfacial area and activities, the mass and heat transfer coefficients are of great importance in the reduction model. For each phase only one mass transfer coefficient as well as heat transfer coefficient was determined.

By definition, the mass transfer coefficient for the steel phase can be expressed as:

$$h_L = \frac{Sh D_L}{L_c}, \quad (81)$$

where Sh is the Sherwood number, L_c is the characteristic length and D_L is the mass diffusivity of steel. As for the characteristic length, the obvious choice was the average slag droplet diameter d_{Aver} . The Sherwood number was determined by using Eq. 82-83 derived by Ihme *et al.* [15]:

$$Sh = 2 + z_k \frac{(ReSc)^{1.7}}{(1 + ReSc)^{1.2}} \quad (82)$$

$$z_k = \frac{0.66}{1 + Sc} + \frac{0.79Sc}{Sc^{\frac{1}{6}}(2.4 + Sc)}, \quad (83)$$

where Sc is the Schmidt number and Re is the Reynolds number defined as follows:

$$Re = \frac{uL_c\rho}{\mu} \quad (84)$$

$$Sc = \frac{\mu}{\rho D}. \quad (85)$$

Eq. 82 has been reported to apply to the entire range of Reynolds numbers. In addition, according to Oeters [6], if the viscosity of the dispersed phase is much greater than the viscosity of the surrounding phase (i.e. $\mu_S \gg \mu_L$) the mass transfer is determined as in the case of mass transfer at solid particles. With steel and slag, the condition is satisfied since the viscosity of slag is typically at least two orders of magnitude greater than that of steel. The model proposed by Ihme *et al.* is applicable specifically for describing the external mass transfer of solid particles and, thus, is a suitable choice in our case.

Due to the fact that the slag viscosity exceeds the steel viscosity to a large extent, mass transfer within the droplets is performed solely by diffusion. The model proposed by Newman [14] was applied for the internal mass transfer. Eq. 86, which gives the Sherwood number for a spherical particle or droplet, has been derived from Fick's second law of diffusion in spheres of finite size. According to Oeters [6] the spherical shape is an acceptable assumption resulting in only small errors. In addition, Oeters emphasizes that diffusion has to be taken into account in the case of emulsified droplets of CaO-Al₂O₃ and CaO-Al₂O₃-SiO₂ slags. Hence, the Sherwood number is given by:

$$Sh = \frac{2\pi^2 \sum_{i=1}^{\infty} \exp(-i^2\pi^2 Fo_m)}{3 \sum_{i=1}^{\infty} \frac{1}{i^2} \exp(-i^2\pi^2 Fo_m)}, \quad (86)$$

where Fo_m is the Fourier number for the mass transfer defined as

$$Fo_m = \frac{4D_{St}}{d_{Aver}^2}. \quad (87)$$

Eq. 86 is time-dependent. It can be proven that the right hand side of the equation approaches $\frac{2\pi^2}{3}$ as $t \rightarrow \infty$.

As for the gas phase, the role of the mass transfer within the gas phase is not highly significant in the slag reduction because the conditions for the formation of CO are not favourable. Thus, the formation of CO, although included in the model, does not have a great effect on the reduction reactions. Regardless, the surface renewal model by Higbie [16] was applied to describe the gas side mass transfer:

$$Sh = 2 + \frac{2}{\sqrt{\pi}} \sqrt{ScRe} = 2 + \frac{2}{\sqrt{\pi}} \sqrt{\frac{d_b u_b}{D_G}}, \quad (88)$$

where u_b and d_b are the rising velocity and diameter of gas bubbles, respectively. These quantities can be evaluated according to the following equations [6]:

$$d_b = \sqrt[3]{\frac{3\sigma d}{g\rho_L} + \sqrt{\frac{9\sigma^2 d^2}{g^2 \rho_L^2} + K \frac{\dot{V}_G^2 d}{g}}} \quad (89)$$

$$u_b = \sqrt{\frac{2\sigma}{\rho_L d_b} + \frac{g d_b}{2}}, \quad (90)$$

where σ is the surface tension, d is the nozzle diameter, \dot{V}_G^2 is the volumetric gas flow rate and $K = 10$ is a experimentally determined constant. x

For determining the heat transfer coefficients, the analogy between mass and heat transfer was applied. The heat transfer coefficient, α , is obtained using the following equation:

$$\alpha = \frac{Nuk}{L_c}, \quad (91)$$

where Nu is the Nusselt number and k is the heat conductivity. In the case of steel and gas heat transfer coefficients, the equations for Nu are similar to the respective Sherwood number equations except that the Schmidt number is replaced with the Prandtl number, Pr . The Prandtl number is defined as follows:

$$Pr = \frac{c_p \mu}{k}. \quad (92)$$

As for the heat transfer coefficient for slag, Nu is obtained from Eq. 86 by replacing Fo_m by Fo_h , the Fourier number of heat transgfer which is, in the case of a slag droplet, defined as:

$$Fo_h = \frac{4kt}{\rho_S c_{p,S} d_{Aver}^2}. \quad (93)$$

Thus, the heat transfer coefficient for steel, slag and gas phases are determined from Eq. 94, 95 and 96, respectively, as follows:

$$Nu = 2 + \left(\frac{0.66}{1 + Pr} + \frac{0.79Pr}{Pr^{\frac{1}{6}}(2.4 + Pr)} \right) \frac{(RePr)^{1.7}}{(1 + RePr)^{1.2}} \quad (94)$$

$$Nu = \frac{2\pi^2 \sum_{i=1}^{\infty} \exp(-i^2\pi^2 Fo_h)}{3 \sum_{i=1}^{\infty} \frac{1}{i^2} \exp(-i^2\pi^2 Fo_h)} \quad (95)$$

$$Nu = 2 + \frac{2}{\sqrt{\pi}} \sqrt{PrRe}. \quad (96)$$

4.2.5 The physical properties of the phases

Models for determining physical properties, i.e. densities and viscosities, of steel, slag and gas were taken from the literature. The following temperature dependent equation derived by Brandes and Brook [53] was applied for updating the density of the steel phase:

$$\rho_L = \rho^* + (T - T^*) \frac{d\rho}{dT}, \quad (97)$$

where $\rho^* = 7015 \text{ kg/m}^3$ is density of pure iron at its melting point $T^* = 1809.4 \text{ K}$ is the melting point and $\frac{d\rho}{dT} = -0.883 \text{ kg/(K}\cdot\text{m}^3)$.

The density of the slag is defined as a function of composition but it does not take the temperature into account. The density of slag is evaluated with the following formula [54]:

$$\rho_S = \frac{\sum_i x_i M_i}{\sum_i x_i V_i}, \quad (98)$$

where x_i , M_i and V_i are the mole fraction, molar mass and molar volume of slag species i , respectively. Molar volumes for the relevant species are given in Table 6.

Table 6. Molar volumes for the slag species at 1773 K. [54]

Species	V_i [cm ³ mol ⁻¹]
Al ₂ O ₃	$28.31 + 32x_{\text{Al}_2\text{O}_3} - 31.45x_{\text{Al}_2\text{O}_3}^2$
SiO ₂	$19.55 + 7.966x_{\text{SiO}_2}$
CaO	20.7
FeO	15.8
MnO	15.6

The viscosity of molten steel was calculated using Eq. 99:

$$\mu_L = \mu_0 \exp \frac{E}{RT}, \quad (99)$$

where $\mu_0 = 0.0003699$ Pa·s and $E = 41400$ J/mol are constants experimentally defined for pure iron, and $R = 8.3144$ J/(K·mol) is the gas constant [53].

As for the viscosity of slag, the modified Urbain model proposed by Kondratiev and Jak [13] was applied. The model is based on the Weymann-Frenkel equation which was modified by Urbain [55]:

$$\mu = AT \exp \left(\frac{1000B}{T} \right), \quad (100)$$

where $-\ln A = mB + n$. The unit of Eq. 100 is Poise. Parameters A and B are composition dependent, whereas m and n are empirical parameters. Parameter m is given by:

$$m = m_A X_A + m_C X_C + m_F X_F + m_S X_S, \quad (101)$$

where X_A , X_C , X_F and X_S are the molar fractions of Al₂O₃, CaO, FeO and SiO₂, respectively.

Parameter B is defined as follows:

$$B = \sum_{i=0}^3 b_i^0 X_S^i + \sum_{i=0}^3 \sum_{j=1}^2 \left(b_i^{c,j} \frac{X_C}{X_C + X_F} + b_i^{f,j} \frac{X_F}{X_C + X_F} \right) \alpha^j X_S^i \quad (102)$$

$$\alpha = \frac{X_C + X_F}{X_C + X_F + X_A}. \quad (103)$$

The terms in 101 and 103 are given in Table 7.

Table 7. Viscosity model parameters.

j/i	0	1	2	3			
b_i^0	0	13.31	36.98	-177.70	190.03	n	9.322
$b_i^{C,j}$	1	5.50	96.20	117.94	-219.56	m_F	0.665
	2	-4.68	-81.60	-109.80	196.00	m_C	0.587
$b_i^{F,j}$	1	34.30	-143.64	368.94	-254.85	m_A	0.370
	2	-45.63	129.96	-210.28	121.20	m_S	0.212

4.2.6 Validation of the models

It is quite obvious that validation of such mathematical slag emulsification models that concern real slag and steel systems is a very challenging task as in the real process the emulsification phenomena cannot be monitored. As far as the author is aware, only experimental data from a ladle process concerning slag emulsification has been presented by Lachmund *et al.* [11]. Obtaining reliable industrial data would require an extensive experimental campaign and that would have been impossible to carry out within the framework of this study. Naturally, mathematical models based on physical modelling can be validated. In PAPER I the oil-water experiments that were carried out by Savolainen *et al.* [5] were modelled with CFD. The results differed somewhat from the experimental data in that the CFD model gave smaller average droplet sizes than were measured from the physical model. The same trend recurred in the CFD study by Senguttuvan *et al.* [33] in which some of the cases carried out by Savolainen *et al.* were simulated. In the study it was suspected that the reason for the difference was the fairly small sample of measured droplets. In PAPER III, in which slag-steel cases were simulated, the results were compared to the model developed by Oeters and qualitatively compared to the study by Lachmund *et al.*

For validating the slag reduction model, a specific validation campaign was arranged in the SSAB Raahe steel plant. Measurements in the CAS-OB station were carried out by a specialized sampler group. In the campaign, slag and steel samples as well as temperature measurements were taken from three stages during the process: 1) before heating stage when the ladle came to CAS-OB station, 2) after the heating

stage just before the bottom stirring for slag reduction was started and 3) after the slag reduction. The samples and measurements were taken with standard process measurement equipment. Steel and slag samples were taken using a lollipop sampler and the samples were sent for analysis. Steel composition was determined by optical emission spectrometry (OES) and the slag composition was determined by X-ray diffraction (XRD). Temperature measurements were carried out by applying immersion thermocouples.

During the validation campaign, samples and temperature measurements were taken from eight heats. In addition to the previously mentioned measurements, essential process data required by the model and other observations were recorded. Slag and steel compositions and temperatures from between the heating and reduction stages was applied as the initial values in the model. The calculated results were compared to final compositions and temperatures. The results predicted by the model proved to be in fairly good agreement with the validation data. The validation results are represented in more detail in the following chapter.

5 Results and discussion

The main results from the original papers are summarised in this chapter. First the results of the emulsification studies (PAPER I-III) are presented with discussion. Finally, the main results of the thesis, i.e. the results given by the slag reduction model are given with some further discussion.

5.1 Slag emulsification

5.1.1 *The effect of physical properties*

In PAPER I the focus of the study was on the droplet size. The effect of different physical properties of slag and steel on the average droplet size and droplet size distribution was studied. To avoid confusion, in the following the cases are denoted as "Case case number/paper number", e.g. Case 2/II is the case number 2 in PAPER II. Four oil-water systems and three slag-steel systems were simulated in the study (Case 1/I-4/I). The oil-water systems were selected from the study by Savolainen *et al.* [5]. The oil layer width in the selected cases were 5 mm or 15 mm and two cases with each layer width were simulated. Two different oils were applied. Simulations were carried out with 5 mm and 15 mm thicknesses for each oil in order to simulate the effect of slag layer thickness. The inlet velocities, i.e. the critical velocities, and interfacial tensions were obtained from the measurements carried out by Savolainen *et al.* The density and viscosity of water were constant, 997 kg/m^3 and $0.88 \text{ mPa}\cdot\text{s}$, respectively.

In the slag-steel cases (Case 5/I-7/I) the main focus was on the effect of the interfacial tension on the droplet size. The viscosity of the slag and steel was constant, 2650 and 6800 kg/m^3 , respectively. Also the viscosity of slag and steel was constant, 0.18 and $0.0049 \text{ Pa}\cdot\text{s}$, respectively. The properties used in each case are collected in Table 8.

Table 8. Properties of the simulated cases in PAPER I.

	Case 1/I	Case 2/I	Case 3/I	Case 4/I	Case 5/I	Case 6/I	Case 7/I
Oil/slag width [mm]	5.0	5.0	15.0	15.0	15.0	15.0	15.0
Interfacial tension [N/m]	0.01304	0.01295	0.01304	0.01295	0.5	0.75	1.05
Viscosity [Pa·s]	0.06134	0.14980	0.06134	0.14980	0.18	0.18	0.18
Density difference [kg/m ³]	94.0	130.0	94.0	130.0	4150.0	4150.0	4150.0
Water/steel velocity [m/s]	0.285	0.361	0.324	0.444	0.18	0.18	0.18

It appeared that the CFD model presented in PAPER I predicted smaller droplet diameters compared to other studies and models as it can be seen from Table 9.

Table 9. Simulated average droplet diameters in millimeters and comparison with the literature.

	PAPER I	Oeters [6]	Asai [56]	Savolainen <i>et al.</i> [5]
Case 1/I	2.78	6.50	13.03	6.75
Case 2/I	2.95	5.50	11.04	7.50
Case 3/I	3.06	6.50	13.03	8.22
Case 4/I	3.13	5.50	11.04	8.50
Case 5/I	3.12	6.10	12.14	-
Case 6/I	3.38	7.50	14.87	-
Case 7/I	3.63	8.80	17.59	-

As mentioned in Section 3.1.2, some of the simulated cases presented in Table 9 were re-simulated by Senguttuvan *et al.* [33]. Comparison of the results by Savolainen *et al.*, Senguttuvan *et al.* and results from PAPER I are given in Table 10. As in PAPER I, they compared the average droplet size obtained from the CFD model to the average droplet size measured from the physical model and found that the droplet size predicted by the computational model was somewhat smaller. A supposed reason for this was a quite small sampling of the measured droplets, 10-20 droplets, from the physical modelling.

Table 10. Comparison of the results [33].

	Mean droplet diameter [mm]		
	Senguttuvan <i>et al.</i> [33]	Savolainen <i>et al.</i> [5]	PAPER I
Oil-water			
Case 2/I	4.53	8.22	2.95
Case 4/I	5.56	8.50	3.13
Steel-slag			
Case 5/I	4.43	-	3.12
Case 7/I	4.70	-	3.63

5.1.2 The effect of interfacial tension

In PAPER II further investigations were carried out on the effect of interfacial tension on the slag emulsification. A similar computational domain as in PAPER I was applied in the study with the exception that the grid was much denser, consisting of over 2 million cells. Three cases (Case 1/II-3/II) were simulated. Properties used in the simulations are collected in Table 11.

Table 11. Properties of simulated cases in PAPER II.

	Case 1/II	Case 2/II	Case 3/II
Interfacial tension [N/m]	0.5	0.75	1.0
Inlet velocity [m/s]	0.5	0.5	0.5
	Steel	Slag	Gas
Density [kg/m ³]	6800	2650	1.51
Viscosity [Pa·s]	0.049	0.3	1.865·10 ⁻⁵

The results show that droplet size increases with increasing interfacial tension. The emulsification fraction decreases when the interfacial tension is increased. The inlet velocity is quite low, 0.5 m/s, and it produces merely moderate emulsification and also the droplet size is quite large for such a flow velocity. The results are presented in Fig. 20 (a)-(d).

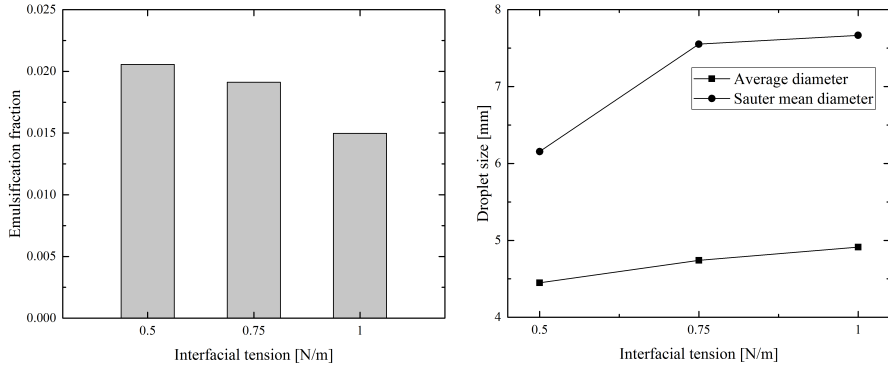


Fig. 20. Emulsification fraction (left) and droplet size (right) as a function of interfacial tension.

5.1.3 The effect of steel flow velocity

In PAPER III the effect of steel flow velocity on slag emulsification was studied. Simulations were carried out in computational grids of two different densities, the first one consisting of over 2 million cells and the other over 4 million cells. Three inlet velocities were applied in the simulations: 0.4, 0.5 and 0.6 m/s. The physical properties were the same as in Table 11 except for slag density which was 2750 kg/m^3 . According to the information obtained from the steel plant, the chosen value for the density corresponds to the slag in the CAS-OB process. The slag layer width in this study was 15 mm. Savolainen *et al.* [5] concluded that using the Weber number did not give sufficient criterion for the emulsification. The insufficiency of the criterion was noted in PAPER III as well, in which in a system where $We = 8.84$, emulsification occurred.

Again size distributions and the average size of droplets were investigated. The computational grid sets a limit on smallest possible droplet size that can be detected in the domain. This is not necessarily the smallest droplet size that occurs in reality under similar conditions. In other words, it is possible that the total range of size distribution is not fully obtained with the model. Therefore, Rosin-Rammler-Sperling distribution functions were fitted to the simulation data. This method was adopted in order to simulate the fraction of droplets that cannot be detected with the CFD model, i.e. the smallest droplets. The simulation data and fitted RRS curves are presented in Fig. 21

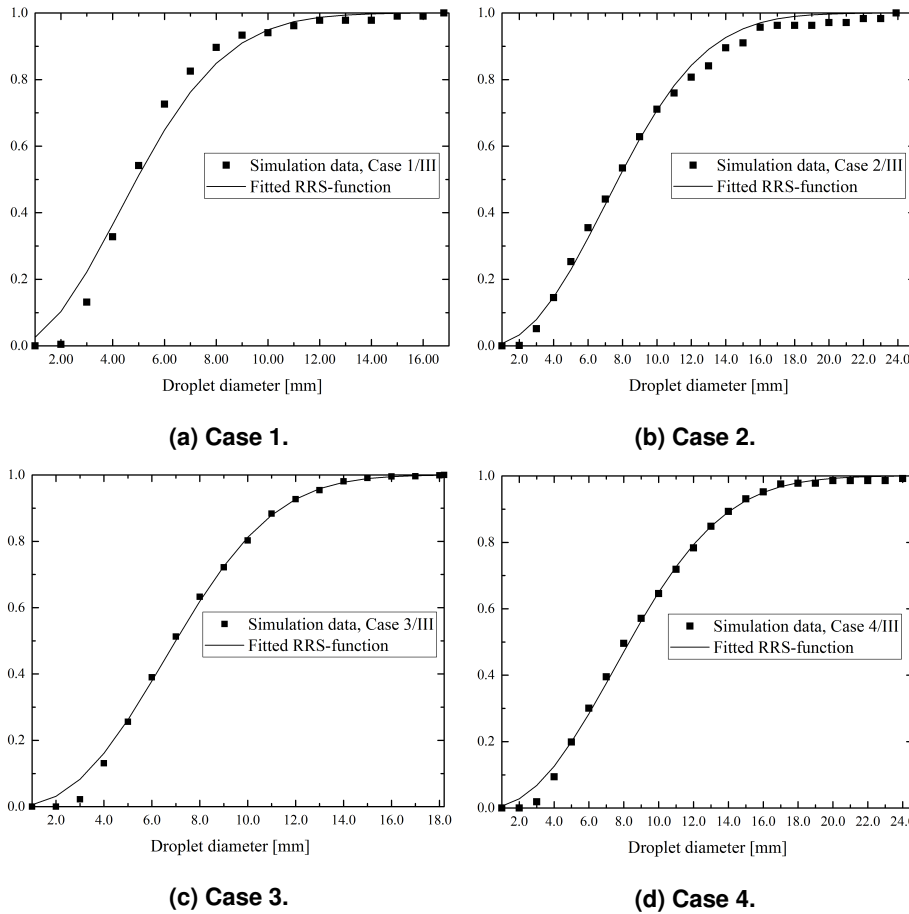
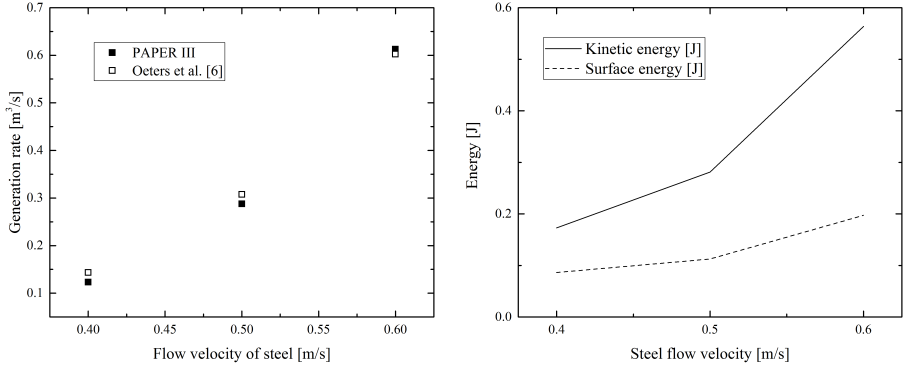


Fig. 21. Simulation data and fitted RRS-functions in Case 1-4.

In addition, the volumetric and area generation rates were done based on estimations from the obtained RRS-functions. The volumetric generation rate according to the simulations was compared to the generation rate equation given by Oeters' model [6] which can be derived from Eq. 16. The results were found to be very similar, as can be seen from Fig 22 (a). Furthermore, in order to verify that the energy that is put into the system really enables droplet formation, the kinetic energy and surface energy of droplets were compared. The result can be seen in Fig. 22 (b).

As mentioned earlier, the validation of computational emulsification models is very difficult when slag-steel systems are concerned. Obviously, as the phenomenon



(a) Volumetric generation rate, (b) Kinetic energy and surface energy as a function of droplet formation. Oeters' model [6].

Fig. 22. Generation rate and energy in the studied system.

cannot be visually observed the measurements should be carried out by taking samples from the steel during bottom blowing and analysing the slag droplets from the samples. This is extremely complicated and would require extensive and exceptional validation arrangements because this cannot be carried out using ordinary process measurement equipment. Moreover, even though the samples would certainly provide valuable data from actual process it is unclear how well the samples would represent the actual dynamic situation.

The studies carried out in PAPER I and II form a preliminary basis towards an applicable emulsification model which was developed in PAPER III and applied in PAPER IV. The results from PAPER I-II were not applied in the reduction model of the CAS-OB process directly. The simulations in PAPER I were carried out in a coarser grid than the later simulations. The grid density plays a very important role in modelling of emulsification. Since the diameter of the slag droplets is typically in the order of millimeters, the grid cells must be very small as well so that the droplets can be detected. In PAPER I and II, the criterion was that droplets containing at least one cell full of slag phase, i.e. the volume fraction of slag phase in the cell was 1, were taken into account. In paper III a more stringent criterion was applied. That is, the droplet diameter, d , must satisfy the following condition:

$$d \geq 2\Delta x = \lambda_{Nyq}, \quad (104)$$

where Δx is the cell size. I.e. droplet for which the diameter was larger than the Nyquist wavelength, λ_{Nyq} , were taken into account.

The approach that was adopted in PAPER I-III, i.e. employing a VOF-LES simulation in a restricted domain and tracking the droplets in the post-processing stage, has been recently applied by Senguttuvan *et al.* and Huang *et al.* [33, 35].

5.2 The reduction stage model

5.2.1 Steel and slag compositions

Slag and steel compositions were predicted for eight heats and the results were compared to the data obtained in the validation campaign. Gas flow rates with exact timing needed in the model were obtained from the process data from the steel plant. Since the effect of CaO on the activities of the slag species is taken into account in the model, the amount of calcium needed to be calculated. This was done according to the process data from the preceding BOF converter process where the calcium additions are made before the ladle is transported to the CAS-OB station. CaO is included in multiple additions, such as dolomite, bauxite etc. The total amount of CaO was calculated as a sum of the product of the mass and CaO content of each CaO containing addition. With the exception of aluminium for heating, no further additions were made in the CAS-OB station to any of the heats.

All cases were calculated using a timestep of one second. The total duration of the reduction treatment from each heat was timed during the validation campaign, starting from the first measurement, or sampling, between heating and reduction stages, and ending with the final temperature measurement after the reduction which was always the last measurement.

Predicted and measured end-compositions have been collected into Tables 12 and 13. As for the steel composition, the results were found to be satisfactory. The mean absolute errors (MAE) for Al, Si, Mn and C were 0.004 wt-%, 0.008 wt-%, 0.03 wt-% and 0.001 wt-%, respectively. The MAEs for the end-content of Al_2O_3 , SiO_2 , CaO, MnO and FeO were 1.2 wt-%, 0.7 wt-%, 1.5 wt-%, 1.7 wt-% and 0.7 wt-%, respectively.

Table 12. Measured and predicted steel compositions.

Heat	Type	Al	Si	Mn	C	Heat	Type	Al	Si	Mn	C
1	Initial	0.04	0.10	1.25	0.05	5	Initial	0.05	0.16	0.59	0.10
	Final	0.03	0.09	1.31	0.05		Final	0.04	0.14	0.60	0.10
	Model	0.03	0.10	1.27	0.05		Model	0.02	0.14	0.66	0.10
2	Initial	0.04	0.12	1.28	0.05	6	Initial	0.06	0.16	0.60	0.10
	Final	0.04	0.12	1.30	0.05		Final	0.04	0.19	0.68	0.10
	Model	0.04	0.12	1.29	0.05		Model	0.05	0.15	0.62	0.10
3	Initial	0.04	0.11	1.25	0.05	7	Initial	0.05	0.01	0.36	0.04
	Final	0.04	0.11	1.24	0.05		Final	0.04	0.01	0.38	0.04
	Model	0.03	0.11	1.27	0.05		Model	0.04	0.01	0.37	0.04
4	Initial	0.06	0.12	1.31	0.05	8	Initial	0.03	0.19	0.68	0.10
	Final	0.05	0.12	1.36	0.05		Final	0.03	0.20	0.69	0.10
	Model	0.05	0.12	1.33	0.05		Model	0.03	0.19	0.68	0.10

The comparison between the predicted and measured concentrations of dissolved species is illustrated in Fig. 23 (a). The predicted slag compositions were not as accurate but still satisfactory. The comparison between the measured and predicted slag composition is presented in Fig. 23 (b).

The results regarding the heat transfer were validated using the measured steel temperatures. The measurement taken before the reduction stage served as an initial condition and it was assumed that all phases have the same temperature at the beginning. The factors affecting the total heat transfer in the system consisted of the heat transfer between the phases, heat losses through the ladle wall and slag-steel surface, as well as the heat consumed/produced by the chemical reactions. Furthermore, it was assumed that the heat that was consumed was taken from the steel. Measured initial and final temperatures, as well as the final temperatures predicted by the model are presented in Table 14. The mean absolute error for the data in Table 14 was 4 °C which can be considered fairly good accuracy. The comparison between the measured and predicted temperatures are presented in Fig. 24 (a). Fig. 24 (b) illustrates the heat losses in

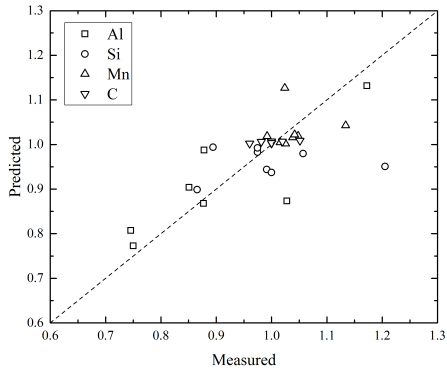
Table 13. Measured and predicted slag compositions.

Heat	Type	Al ₂ O ₃	SiO ₂	CaO	MnO	FeO	Heat	Type	Al ₂ O ₃	SiO ₂	CaO	MnO	FeO
1	Initial	32.09	14.00	46.62	6.12	1.18	5	Initial	39.92	13.81	30.08	8.57	7.63
	Final	35.04	16.39	45.72	2.37	0.49		Final	43.49	17.50	31.08	6.57	1.35
	Model	34.11	14.34	47.38	3.49	0.67		Model	45.77	16.90	32.03	2.81	2.49
2	Initial	30.34	12.40	54.59	1.97	0.70	6	Initial	39.82	10.61	35.17	5.73	8.67
	Final	31.21	12.94	54.59	0.81	0.45		Final	40.70	12.44	39.39	5.07	8.67
	Model	30.59	12.88	54.86	1.23	0.44		Model	43.16	12.44	36.51	3.14	4.75
3	Initial	33.44	11.00	44.98	6.69	3.90	7	Initial	44.88	4.75	41.01	5.28	4.08
	Final	35.02	11.85	42.99	7.79	2.34		Final	43.86	4.54	41.42	5.43	4.74
	Model	34.88	12.37	45.96	4.30	2.50		Model	46.03	4.88	41.34	4.37	3.39
4	Initial	35.83	12.23	45.14	5.59	1.20	8	Initial	31.50	12.49	54.71	0.67	0.63
	Final	37.43	13.37	42.82	5.57	0.80		Final	32.22	12.51	54.47	0.46	0.34
	Model	37.50	12.56	45.75	3.46	0.74		Model	30.67	13.56	54.82	0.49	0.45

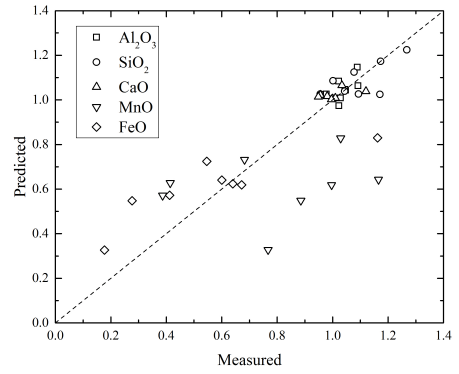
Heat 3. As it can be seen, most heat is lost by radiation through the surface. Bottom stirring breaks the slag and exposes molten steel to the atmosphere, and in the absence of insulation provided by the top slag a considerable amount of heat is lost. The endothermic reduction reactions absorb heat. It can be seen that at the beginning of the reduction the reactions consume heat faster, resulting in faster cooling of the steel. Furthermore, heat is obviously lost through the ladle walls as well. In Fig. 24(b) a positive sign is assigned if heat is given out and a negative sign if heat is consumed.

Table 14. Measured and predicted steel temperatures.

Heat/Type	1	2	3	4	5	6	7	8
Initial	1604	1619	1599	1598	1616	1617	1623	1591
Final	1595	1606	1589	1588	1600	1587	1610	1578
Model	1593	1608	1588	1587	1600	1602	1617	1582

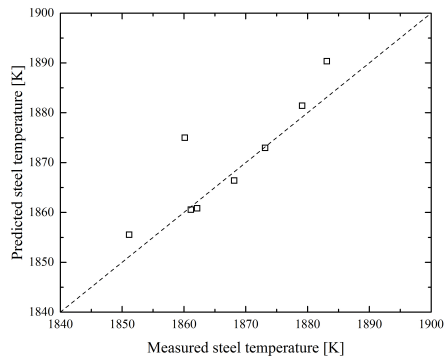


(a) Steel composition, measured versus predicted.

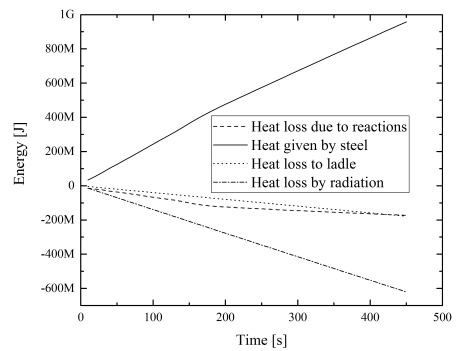


(b) Slag composition, measured versus predicted.

Fig. 23. Steel and slag compositions.



(a) Steel temperature, measured versus predicted.



(b) Heat losses in Heat 3.

Fig. 24. Steel temperatures and heat losses predicted by the model.

6 Conclusions and future work

Novel models for modelling the emulsification of slag and slag reduction in a CAS-OB process were presented in this dissertation. The emulsification of slag was studied by means of CFD simulations. In PAPER I, the effect of the slag layer width, interfacial tension between the slag and steel and the viscosity of the slag on the average droplet size and droplet size distribution was examined. The study consisted of four oil-water cases and three slag-steel cases. The simulation results were compared to results found in the literature and it was concluded that the CFD model predicted smaller droplet sizes than in those studies. This study formed the basis for the following CFD studies. PAPER II concerned the effect of interfacial tension on the emulsification. In distinction to PAPER I, the simulations were carried out in significantly denser grid. Three cases were simulated using an interfacial tension of 0.5, 0.75 and 1.0 N/m. By varying the interfacial tension it was attempted to simulate the effect of chemical reactions on the emulsification. It was found out that the average droplet size increases with the interfacial tension. Another observation was that the emulsification fraction increased when the interfacial tension was decreased. PAPER III focused on the effect of the flow velocity of steel on the emulsification. Three cases were simulated using three different flow velocities, 0.4, 0.5 and 0.6 m/s. Dense grids were used in the simulations. Rosin-Rammler-Sperling distribution functions were fitted to the droplet size distribution data obtained from the model. Based on the obtained distribution functions, volumetric and interfacial area generation rates were determined. The volumetric generation rates were found to agree well with Oeters' theory. The generation rate of interfacial area was found to be in good relation with the results of the Lachmund study.

In PAPER IV, a new mathematical model for the reduction stage of the CAS-OB process was presented. The main task was to model the chemical reactions and heat transfer during the reduction. In developing the model it was assumed that the reactions are mass transfer limited due to high temperatures in the process and, thus, the reaction rates could be formulated by employing the Modified Law of Mass Action approach. Droplet generation has a significant role in enhancing the mass transfer between slag and steel during reduction. The results obtained in PAPER I-III were exploited to describe the amount of the interfacial area in the reduction stage model. Numerous submodels were employed for modelling heat and mass transfer coefficients, activities of slag and

steel species, slag viscosity, open-eye diameter etc. The model was validated by data obtained from eight heats in a validation campaign at SSAB Raahe. It was concluded that the model predictions were in good agreement with the validation data. The mean absolute errors (MAE) for Al, Si, Mn and C were 0.004 wt-%, 0.008 wt-%, 0.03 wt-% and 0.001 wt-%, respectively. The MAEs for the end-content of Al_2O_3 , SiO_2 , CaO, MnO and FeO were 1.2 wt-%, 0.7 wt-%, 1.5 wt-%, 1.7 wt-% and 0.7 wt-%, respectively. The MEA for the predicted steel temperature was 4 °C. Furthermore, it was noticed that during the reduction most of the heat was lost through radiation from the slag-steel surface. Other significant factors affecting the cooling were heat consuming reduction reactions and heat losses through the ladle wall.

This study presents a functional, fast model for simulating the reduction stage of the CAS-OB process that was developed by way of mathematical reaction modelling and CFD modelling. The results were in good agreement with the experimental measurements. Furthermore, the model gives a good basis for developing process models for similar processes.

As for the future work, the development of the model continues with combining the heat-up stage model and reduction stage model to form a CAS-OB simulator. For the end-user friendliness, implementing a graphical user interface (GUI) for the simulator is also essential. The main aim would be a CAS-OB process simulator that can be used as a development and optimization tool in industrial environments. Another possible task in the future is to extend the reduction model for processes in which the emulsification phenomenon plays an important role, e.g. desulphurization.

References

1. Cramb A & Jimbo I (1989) Calculation of Interfacial Tension in Metal-Slag Systems. *Steel Res.* 60(3/4): 157–165.
2. Mietz J, Schneider S & Oeters F (1991) Model Experiments on Mass Transfer in Ladle Metallurgy. *Steel Res.* 62(1): 1–9.
3. Mietz J, Schneider S & Oeters F (1991) Emulsification and Mass Transfer in Ladle Metallurgy. *Steel Res.* 62(1): 10–15.
4. Harman J & Cramb A (1996) A Study on the Effect of Fluid Physical Properties on Droplet Emulsification. In: *Steelmaking Conference Proceedings*, volume 79, pp. 773–784.
5. Savolainen J, Fabritius T & Mattila O (2009) Effect of Fluid Physical Properties on the Emulsification. *ISIJ Int.* 49(1): 29–36.
6. Oeters F (1989) *Metallurgy of Steelmaking*. Verlag Stahleisen mbH.
7. Sulasalmi P, Kärnä A, Fabritius T & Savolainen J (2009) CFD Model fo Emulsification of Slag into the Steel. *ISIJ Int.* 49(11): 1661–1667.
8. Sulasalmi P, Visuri VV & Fabritius T (2013) Effect of Interfacial Tension on the Emulsification of Slag– Considerations on the CFD Modelling of Dispersion. *Mater. Sci. Forum* 72: 242–247.
9. Sulasalmi P, Visuri VV, Kärnä A & Fabritius T (2015) Effect of Interfacial Tension on the Emulsification of Slag– Considerations on the CFD Modelling of Dispersion. *Steel Res. Int.* 85(3): 212–222.
10. Cramb A, Chung Y, Harman J, Sharan A & Jimbo I (1997) The Slag Metal Interface and Associated Phenomena. In: *International Slag Symposium Proceedings*, pp. 35–50.
11. Lachmund H, Xie Y, Buhles T & Pluschke W (2003) Slag Emulsification During Liquid Steel Desulphurisation by Gas Injection into the Ladle. *Steel Res. Int.* 74(2): 77–85.
12. Krishnapisharody K & Irons GA (2008) An Extended Model for Slag Eye Size in Ladle Metallurgy. *ISIJ Int.* 48(12): 1807–1809.
13. Kondratiev A & Jak E (2001) Review of Experimental Data and Modelling of the Viscosities of Fully Liquid Slags in the Al₂O₃-CaO-FeO-SiO₂ Systems. *Met. Trans. B* 32B: 1015–1025.
14. Newman AB (1931) The Drying of Porous Solids: Diffusion and Surface Emission Equations. *Trans. Am. Inst. Chem. Eng.* 27: 203–220.
15. Ihme F, Schmidt-Taub H & Brauer H (1972) Theoretische Untersuchung über die Umströmung und den Stoffübergang an Kugeln. *Chem-Ing-Tech.* 44(5): 306–313.
16. Higbie R (1935) The Rate of Absorbtion of a Pure Gas Into a Still Liquid during Short Periods of Exposure. *Trans. Am. Inst. Chem. Eng.* 31: 365–389.
17. Pelton AD & Bale CW (1986) A Modified Interaction Parameter Formalism for Non-Dilute Solutions. *Met. Trans. A* 17A: 1211–1215.
18. Ban-Ya S (1993) Mathematical Expression of Slag-Metal Reactions in Steelmaking Process by Quadratic Formalism Based on the Regular Solution Model. *ISIJ Int.* 33(1): 2–11.
19. Järvinen M, Visuri VV, Kärnä A, Sulasalmi P, Heikkinen EP, Pääskylä K, de Blasio C & Fabritius T (2014) A Novel Approach for Numerical Modeling of the CAS-OB Process: Process Model for the Heat-Up Stage. *ISIJ Int.* 54(10): 2263–2272.
20. Stolte G (2007) *Secondary Metallurgy - Fundamentals, Processes, Applications*. Verlag Stahleisen GmbH.

21. Tuomikoski S (2009) Kemiällinen lämmitys CAS-OB-prosessilla. Diploma thesis, University of Oulu.
22. Ha CS & Park JM (2008) Start-up and some experiences of CAS-OB at POSCO. *Arch. Metall. Mater.* 53(2): 637.
23. Nilsson L, Andersson K & Lindquist K (1996) The CAS-OB Process in the Steelshop at SSAB Tunnsplat AB Luleå Work. *Scand J. Metall.* 25: 73–79.
24. Ma WJ, Bao YP, Zhao LH & Wang M (2014) Physical Modelling and Industrial Trials of CAS-OB Refining Process for Low Carbon Aluminium Killed Steels. *Ironmak. Steelmak.* 41(8): 607–610.
25. Wang HM, Li GR, Dai QX, Li B, Zhang XJ & Shi GM (2007) CAS-OB Refining: Slag Modification with B₂O₃-CaO and CaF₂-CaO. *Ironmak. Steelmak.* 34(4): 350–353.
26. Kulju T, Ollila S, Keiski RL & Muurinen E (2013) Three Phase CFD-simulation of CAS-OB Ladle. *Mater. Sci. Forum* 762: 248–252.
27. Kim SH & Fruehan RJ (1987) Physical Modeling of Liquid/Liquid Mass Transfer in Gas Stirred Ladles. *Metall. Trans. B* 18B: 381–390.
28. Mietz J & Brühl M (1990) Model Calculation for Mass Transfer with Mixing in Ladle Metallurgy. *Steel Res.* 61(3): 105–112.
29. Froberg M, Gerlach F & Handschuh G (1990) Investigation of Drop-size-distribution and Mass Transfer in Gas-stirred Liquid-liquid Systems. *Steel Res.* 61(4): 151–156.
30. Xiao Z, Peng Y & Liu C (1987) Modelling Study of the Entrapment Phenomena at the Slag-metal Interface in the Gas-stirred system. *Chin. J. Met. Sci. Technol.* 3: 187–193.
31. Khajavi L & Barati M (2010) Cold Model Study of Emulsification Behavior in Bottom Blown Metallurgical Baths Covered with Thick Slag. *ISIJ In.* 50(5): 654–662.
32. Wei T & Oeters F (1992) A Model Test for Emulsion in Gas-stirred Ladles. *Steel Res.* 63(2): 60–68.
33. Senguttuvan A & Irons G (2013) Model Studies on Slag Metal Entrainment in Gas-Stirred Ladles. In: *AISTech2014 Proceedings*, pp. 1453–1464.
34. Irons G, Senguttuvan A & Krishnapisharody K (2015) Recent Advances in the Fluid Dynamics of Ladle Metallurgy. *ISIJ Int* 55(1): 1–6.
35. Huang A, Harmuth H, Doletschek M, Vollmann S & Feng X (2015) Toward CFD Modeling of Slag Entrainment in Gas Stirred Ladles. *Steel Res. Int* 86(12): 1447–1454.
36. Huang A, Vollmann S & Harmuth H (2013) Towards Modeling of Slag Entrainment in Gas Stirred Ladles by LES. In: *STEELSIM 2013 Proceedings*.
37. Brackbill J, Kothe D & Zemach C (1992) A continuum method for modeling surface tension. *J. Comput. Phys.* 100(2): 335–354.
38. Hirt CW & Nichols BD (1981) Volume of Fluid (VOF) Method for the Dynamics of Free Boundaries. *J. Comput. Phys.* 39: 201–225.
39. Sagaut P, Deck S & Terracol M (2006) *Multiscale and Multiresolution Approaches in Turbulence*. Imperial College Press.
40. Sagaut P (2002) *Large Eddy Simulation for Incompressible Flows*. Springer-Verlag Berlin Heidelberg New York.
41. Järvinen M, Pisilä S, Kärnä A, Ikäheimonen T, Kupari P & Fabritius T (2011) Fundamental Mathematical Model for AOD Process. Part I: Derivation of the Modell. *Steel Res. Int.* 82(6): 638–649.
42. Visuri VV, Järvinen M, Sulasalmi P, Heikkinen EP, Savolainen J & Fabritius T (2013) A Mathematical Model for the Reduction Stage of the AOD Process. Part I: Derivation of the

- Model. *ISIJ Int.* 53(4): 603–612.
43. Visuri VV, Järvinen M, Kärnä A, Sulasalmi P, Heikkinen EP, Kupari P & Fabritius T (2016) A Mathematical Model for Reactions during Top-Blowing in the AOD Process: Derivation of the Model. *Met. Trans. B* (?): ?–?
 44. Korja S & Lange K (1984) A New Approach to Investigate the Droplet Size Distribution in Basic Oxygen Steelmaking. *Met. Trans. B* 15B: 109–116.
 45. Krishnapisharody K & Irons GA (2015) A Model for Slag Eyes in Steel Refining Ladles Covered with Thick Slag. *Met. Trans. B* 46B: 191–198.
 46. Krishnapisharody K & Irons GA (2006) Modeling of Slag Eye Formation over a Metal Bath Due to Gas Bubbling. *Met. Trans. B* 37B: 763–772.
 47. Sigworth GK & Elliot JF (1974) The Thermodynamics of Liquid Dilute Iron Alloys. *Met. Sci.* 8: 298–310.
 48. Ma ZT, Ohser J & Janke D (1997) Thermodynamic Treatment of Multicomponent Systems using Interaction Parameters. *Acta Metall. Sin.* 10(5): 375–385.
 49. Lumsden J (1961) *Physical Chemistry of Process Metallurgy, Part I.* Interscience.
 50. Sosinsky DJ & Sommerville ID (1986) The Composition and Temperature Dependence of the Sulfide Capacity of Metallurgical Slags. *Met. Trans. B* 17B: 331–337.
 51. Iguchi Y (1990) The Thermochemistry of Ferrous Melts. In: *Elliot Symposium Proceedings*, pp. 129–147.
 52. Ban-Ya S & Shim JD (1982) Application of the Regular Solution Model for the Equilibrium of Distribution of Oxygen between Liquid Iron and Steelmaking Slags. *Can. Metall. Quart.* 21(4): 319–328.
 53. Brandes E & Brook G (1992) *Smithells Metals Reference Book.* Butterworth-Heinemann Ltd.
 54. Keene BJ & Mills KC Densities of Molten Slags. In: *Eisenhüttenleute VD (ed.) Slag Atlas.* Verlag Stahleisen GmbH.
 55. Urbain G (1987) Viscosity Estimation of Slag. *Steel Res.* 58(3): 111–116.
 56. Asai S (1984) . In: 100th and 101st Nishiyama Memorial Seminar, volume 67, p. 90.

Original publications

- I Sulasalmi P, Kärnä A, Fabritius T & Savolainen J (2009) CFD Model for Emulsification of Slag into the Steel. *ISIJ Int* 42(11): 1661–1667.
- II Sulasalmi P, Visuri V-V & Fabritius T (2013) Effect of Interfacial Tension on the Emulsification of Slag – Considerations on the CFD Modelling of Dispersion. *Mater Sci Forum* 762: 242–247.
- III Sulasalmi P, Visuri V-V, Kärnä A & Fabritius T (2015) Simulation of the Effect of Steel Flow Velocity on Slag Droplet Distribution and Interfacial Area Between Steel and Slag. *Steel Res Int* 86(3): 212–222.
- IV Sulasalmi P, Visuri V-V, Kärnä A, Järvinen M, Ollila S & Fabritius T (2016) A Mathematical Model for the Reduction Stage of the CAS-OB Process. *Metall and Materi Trans B*. DOI: 10.1007/s11663-016-0769-8.

Reprinted with permission from ISIJ International (I), Trans Tech publishing (II) and Wiley (III).

Original publications are not included in the electronic version of the dissertation.

575. Suliman, Isameldin Mohammed (2016) Performance analysis of cognitive radio networks and radio resource allocation
576. Karjalainen, Satu Maaria (2016) Identification of processes leading to long-term wastewater purification in northern treatment wetlands
577. Ohenoja, Markku (2016) Computational methods for exploiting image-based data in paper web profile control
578. Väliheikki, Ari (2016) Resistance of catalytic materials towards chemical impurities : the effect of sulphur and biomaterial-based compounds on the performance of DOC and SCR catalysts
579. Kinnunen, Tuomo (2016) Product management perspectives on stakeholder and business opportunity analyses in the front-end of product creation
580. Heiderscheidt, Elisangela (2016) Evaluation and optimisation of chemical treatment for non-point source pollution control : purification of peat extraction runoff water
581. Su, Xiang (2016) Lightweight data and knowledge exchange for pervasive environments
582. Kaijalainen, Antti (2016) Effect of microstructure on the mechanical properties and bendability of direct-quenched ultrahigh-strength steels
583. Lanz, Brigitte (2016) Compact current pulse-pumped GaAs–AlGaAs laser diode structures for generating high peak-power (1–50 watt) picosecond-range single optical pulses
584. Kähäri, Hanna (2016) A room-temperature fabrication method for microwave dielectric Li_2MoO_4 ceramics and their applicability for antennas
585. Chowdhury, Helal (2016) Data download on the move in visible light communications: design and analysis
586. Kekäläinen, Kaarina (2016) Microfibrillation of pulp fibres : the effects of compression-shearing, oxidation and thermal drying
588. Varjo, Sami (2016) A direct microlens array imaging system for microscopy
589. Haapakangas, Juho (2016) Coke properties in simulated blast furnace conditions : Investigation on hot strength, chemical reactivity and reaction mechanism
590. Erkkilä-Häkkinen, Sirpa (2016) Rakentamisen työturvallisuuteen suhtautuminen toimijoiden kokemuksina

Book orders:

Granum: Virtual book store

<http://granum.uta.fi/granum/>

S E R I E S E D I T O R S

A
SCIENTIAE RERUM NATURALIUM

Professor Esa Hohtola

B
HUMANIORA

University Lecturer Santeri Palviainen

C
TECHNICA

Postdoctoral research fellow Sanna Taskila

D
MEDICA

Professor Olli Vuolteenaho

E
SCIENTIAE RERUM SOCIALIUM

University Lecturer Veli-Matti Ulvinen

E
SCRIPTA ACADEMICA

Director Sinikka Eskelinen

G
OECONOMICA

Professor Jari Juga

H
ARCHITECTONICA

University Lecturer Anu Soikkeli

EDITOR IN CHIEF

Professor Olli Vuolteenaho

PUBLICATIONS EDITOR

Publications Editor Kirsti Nurkkala

